Research paper

Design, synthesis and *in vivo* evaluation of 3-arylcoumarin derivatives of rhenium(I) tricarbonyl complexes as potent antibacterial agents against methicillin-resistant *Staphylococcus aureus* (MRSA)

Sara Nasiri Sovari [a], Sandra Vojnovic [b], Sanja Skaro Bogojevic [b], Aurelien Crochet [a], Aleksandar Pavic [b,**], Jasmina Nikodinovic-Runic [b], Fabio Zobi [a,*]

[a] *Department of Chemistry, University of Fribourg, Chemin Du Musée 10, 1700, Fribourg, Switzerland*
[b] *Institute of Molecular Genetics and Genetic Engineering, University of Belgrade, Vojvode Stepe 444a, 11042, Belgrade 152, Serbia*

A B S T R A C T

We have prepared a series of ten 3-arylcoumarin molecules, their respective *fac*-[Re(CO)$_3$(bpy)L]$^+$ and *fac*-[Re(CO)$_3$(L⌢L)Br] complexes and tested all compounds for their antimicrobial efficacy. Whereas the 3-arylcoumarin ligands are virtually inactive against the human-associated pathogens with minimum inhibitory concentrations (MICs) > 150 μM, when coordinated to the *fac*-[Re(CO)$_3$]$^+$ core, most of the resulting complexes showed remarkable antibacterial potency. Several rhenium complexes exhibit activity in nanomolar concentrations against Gram-positive pathogens such as *Staphylococcus aureus* strains, including methicillin-resistant *S. aureus* (MRSA) and *Enterococcus faecium*. The molecules do not affect bacterial cell membrane potential, but some of the most potent complexes strongly interact with DNA, indicating it as a possible target for their mode of action. *In vivo* studies in the zebrafish model showed that the complexes with anti-staphylococcal/MRSA activity were non-toxic to the organism even at much higher doses of the corresponding MICs. In the zebrafish-MRSA infection model, the complexes increased the survival rate of infected fish up to 100% and markedly reduced bacterial burden. Moreover, all rescued fish developed normally following the treatments with the metallic compounds.

1. Introduction

The increase of antimicrobial resistance (AMR) to current clinical drugs and the lack of new antibiotics to combat emerging resistant strains have become major concerns to human health in this century [1,2]. The AMR crisis involves any class of antibiotics including second- and third-line antibiotics once considered the last resort drugs to tackle common infections, leading to persistence and spreading of multidrug-resistant (MDR) microbes [3]. Consequently, about 10 million deaths caused by infectious diseases treatment failure could be reached in 2050 [4]. Researchers and clinicians are faced with the urgent need to develop novel scaffolds and effective antibacterial drugs to overcome AMR emergence and spreading of MDR strains [5,6]. The opportunistic

human pathogens that exhibit multidrug resistance, like *Enterococcus faecium*, *Staphylococcus aureus*, *Klebsiella pneumoniae*, *Acinetobacter baumannii*, *Pseudomonas aeruginosa*, and *Enterobacter* spp., known as ESKAPE pathogens, are considered as a serious global health issue [7,8]. Among them, methicillin-resistant *Staphylococcus aureus* (MRSA) represents the leading cause of nosocomial and community-acquired infections, being recognized by the World Health Organisation (WHO) as the antibiotic-resistant pathogen of high priority. The bacterium is the principal causal agent of complicated skin and soft tissue infections [9], serious bloodstream infections [10], infective endocarditis, and pneumonia [11,12]. According to the Centers for Disease Control and Prevention (CDC), in 2017 almost 120 000 cases of bloodstream infections were caused by *S. aureus* in the United States, resulting in almost 20 000 deaths [13]. Current clinical therapy for MRSA infections relies on the use of vancomycin and daptomycin as the first-line antibiotics, while linezolid represents the drug of last resort [14]. However, MRSA strains resistant to each of these medicines have already been reported [15], posing a high demand for novel therapeutic

options to combat MRSA-related infections.

For decades, lead structures in the pharmaceutical industry and most antimicrobial compounds developed by medicinal chemists were almost exclusively purely organic compounds. However, studies undertaken in the last 10 years on antimicrobial applications [16–21] of organometallic and inorganic metal complexes of iridium [22–24], ruthenium [25–29], manganese [30–33], and gold [21,34] among others, revealed their strong antimicrobial potency against critical bacterial and fungal pathogens and distinct mechanisms of action. Some of these molecules demonstrated activity in the low micromolar or even nanomolar range with no cytotoxicity or hemolytic activity at much higher concentrations [20,24]. Interestingly, rhenium complexes, mostly explored for their anti-tumor properties, were recently shown to possess promising antibacterial potency [35–41]. In particular, Wenzel, Patra et al. introduced a trimetallic complex comprised of a ferrocenyl (Fc), a cymantrene and a [(dpa)Re(CO)$_5$] residue (dpa = *N,N*-bis(pyridine-2-ylmethyl)prop-2-yn-1-amine) as the main biological active moiety of the construct [36,37]. MIC values of the compound against Gram-positive bacterial strains such as *B. subtilis* and *S. aureus* strains involving *S. aureus* ATCC 43300 (MRSA) were in the range of 1.4–21 μM [36]. Siegmund et al. described a family of antimicrobial *N*-heterocyclic carbene (NHC) *fac*-Re(I)(CO)$_3$ complexes containing unsubstituted benzimidazol-2-ylidene and diimine ligands with MIC values of the complexes between 0.7 and 2 μM against Gram-positive *B. subtilits* and *S. aureus* strains [39]. Recently, Frei et al. reported the synthesis of three rhenium bisquinoline complexes and their light-induced activity against drug-resistant *S. aureus* and *E. coli* strains, with an increase in antimicrobial activity between 4- to 16-fold under photo-irradiation than in the dark [40].

While the metal core is of fundamental importance, the nature and coordination mode of the bound ligands may drastically modulate the overall biological activity (antimicrobial activity and toxicity) of the given complex and thus its therapeutic application. Coumarins are well-known antibacterial candidates [42–48], acting via different mechanisms. These include topoisomerase II DNA (gyrase) [49] or D-alanine-D-alanine ligase (DdlB) [50] inhibition, cell membrane integrity [51], or cytochrome biosynthesis disruption [52]. Coumarins, naturally occurring and/or synthetic, also show remarkable pharmacological properties as anticoagulants [53,54], anti-inflammatory [55], antioxidant [56], antiplatelet [57], anticarcinogenic [58–63] and antifungal agents [64]. Because metal coordination of the established drugs can significantly improve their biological activity [32], we decided to design and synthesize a series of 3-arylcoumarin compounds capable of acting as mono and bidentate ligands for the *fac*-[Re(CO)$_3$(bpy)]$^+$ and the *fac*-[Re(CO)$_3$Br] cores respectively (Fig. 1).

The aim of this study was to investigate the antimicrobial potency of the rhenium complexes and respective ligands against the most prevailing human pathogenic microorganisms and to evaluate their therapeutic potential for possible applications in anti-infective therapy. Accordingly, the series of molecules were tested against Gram-positive and Gram-negative bacterial (*E. faecium*, *S. aureus*, MRSA, *L. monocytogenes*, *P. aeruginosa*) and *Candida* fungal strains (*C. albicans*, *C. glabrata*, *C. krusei* and *C. parapsilosis*). The toxicity of the molecules was evaluated *in vivo* in the zebrafish (*Danio rerio*) model and *in vitro* on human lung fibroblasts (MRC-5 cells). The most promising complexes, showing a large therapeutic window, were also evaluated for their antimicrobial efficacy *in vivo* using the zebrafish-MRSA infection model.
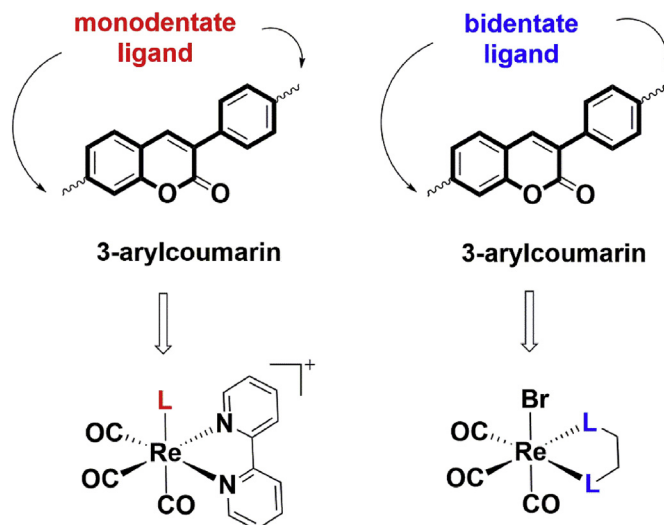

Fig. 1. Simplified representation of 3-arylcoumarin mono and bidentate ligands and their corresponding *fac*-[Re(CO)$_3$]$^+$ complexes (*vide infra* for molecular details).

2. Results and discussion

2.1. Synthesis and characterization of ligands and complexes

The ten 3-arylcoumarin-based ligands were prepared according to the synthetic pathways described in Scheme 1. The synthesis of the 3-arylcoumarin core was achieved by reacting 2-hydroxybenzaldehyde derivatives with 4-halophenylacetic acid by using potassium acetate in acetic anhydride. This step involved sequential acetylation of the hydroxyl groups and pyrone ring closure in a single-pot operation, followed by the hydrolysis of the intermediate using HCl in methanol, which resulted in the main pharmacophore. The following reactions, such as Buchwald–Hartwig amination, etherification, copper-catalyzed azide–alkyne cycloadditions (CuAAC) and *N*-deprotection, were carried out to obtain the series of mono- and bidentate 3-arylcoumarin ligands L$_1$-L$_{10}$ in remarkably high yields (75–95%). Molecules were purified by normal phase column chromatography, fully characterized by ^{1}H NMR (ESI) and ^{13}C NMR spectroscopy, mass spectrometry, IR spectroscopy, and single-crystal X-ray structure analyses (*vide infra*). The ^{1}H NMR spectra of all compounds show a singlet in the range of 8.0–8.5 ppm associated to the pyrone proton of 4-position and confirmed ring closure.
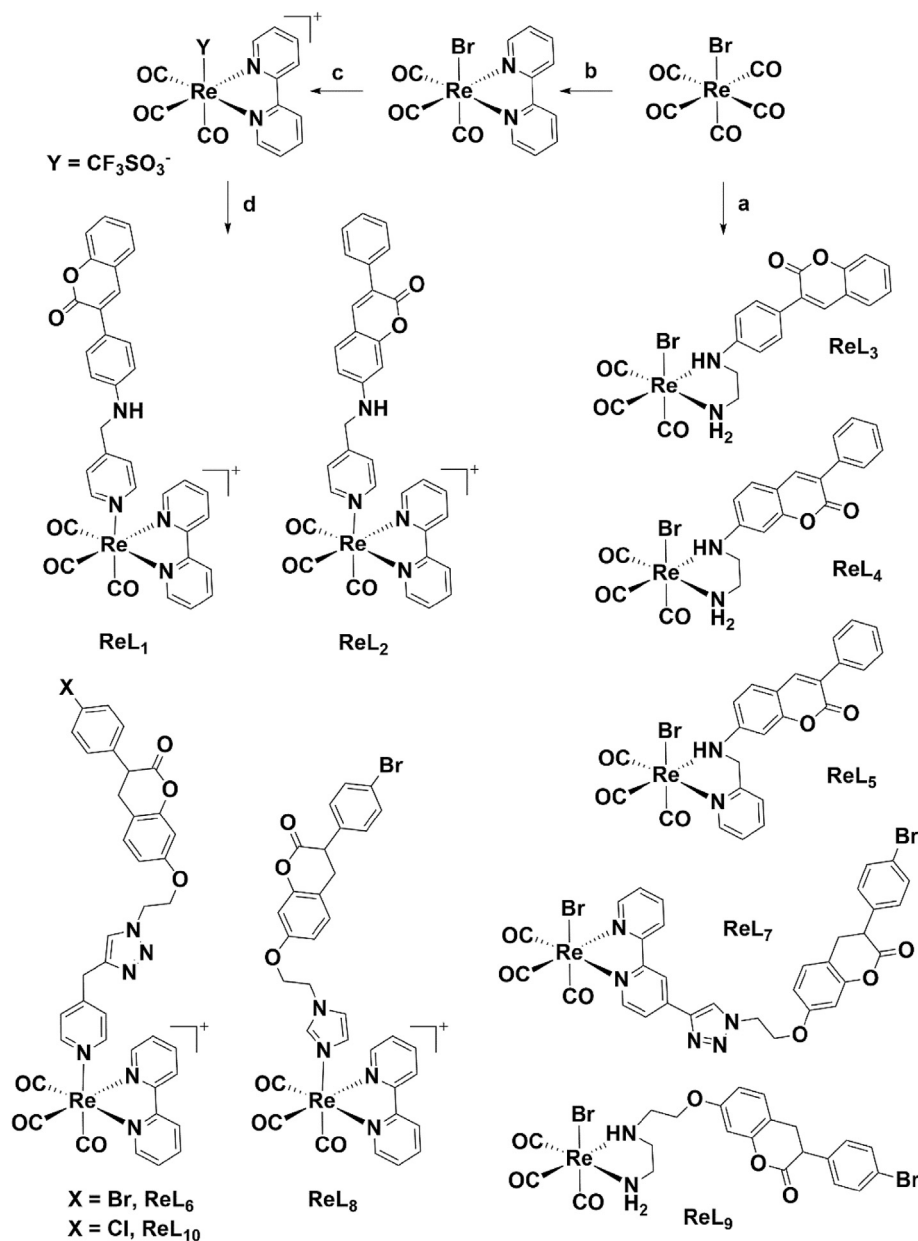
The preparation of rhenium complexes ReL$_1$-ReL$_{10}$ was accomplished via the synthetic protocol illustrated in Scheme 2. A literature procedure was adapted to our needs [65]. A one-step reaction of the bidentate ligands (L$_3$, L$_4$, L$_5$, L$_7$ and L$_9$) with rhenium pentacarbonyl bromide resulted in the desired *fac*-[Re(CO)$_3$(L$_\#$)Br] complexes (where # = 3, 4, 5, 7 and 9). The complexation of 3-arylcoumarin monodentate ligands (L$_1$, L$_2$, L$_6$, L$_8$ and L$_{10}$) to *fac*-[Re(CO)$_3$(bpy)]$^+$ was carried out stepwise by preparation of the *fac*-[Re(CO)$_3$(bpy)Br] complex [66], its activation by bromide exchange with triflate (CF$_3$SO$_3^-$) and final displacement of the anion for the desired monodentate ligands under mild conditions. The cationic *fac*-[Re(CO)$_3$(bpy)L$_\#$]$^+$ species (where # = 1, 2, 6, 8 and 10) were finally isolated as hexafluorophosphate salts by addition of NH$_4$PF$_6$ in methanol. According to the recent definition of Metzler-Nolte and Cohen [67], these complexes belong to the class F metallofragments based-drugs. All rhenium complexes were also characterized by standard techniques including single-crystal X-ray
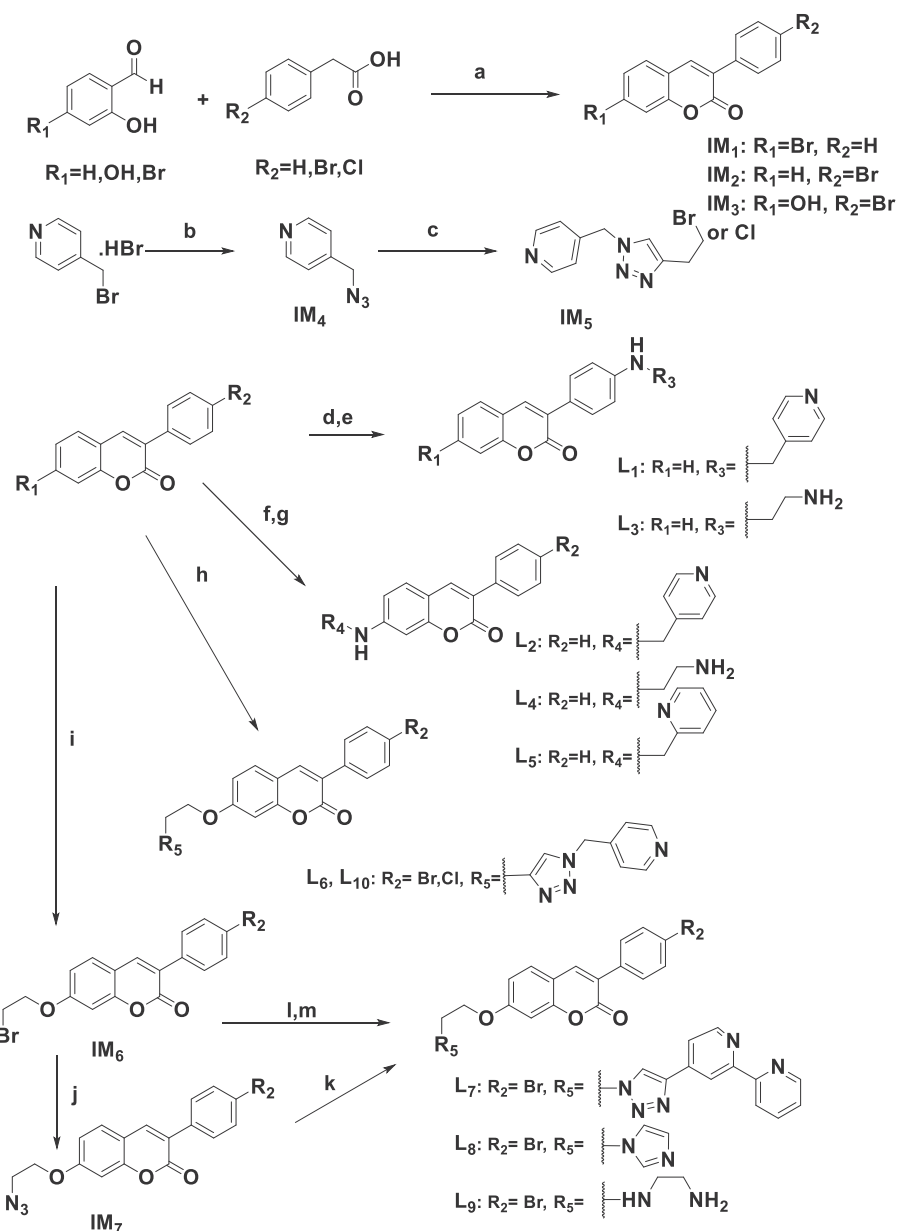
Scheme 1. Synthesis and chemical structures of 3-arylcoumarin ligands (L$_1$-L$_{10}$). Conditions: (a) CH$_3$COOK, Ac$_2$O, at 120 °C 10 h, under argon/HCl 2N, MeOH, reflux, 4 h, 90−95%; (b) 4-(bromomethyl)pyridine.HCl, K$_2$CO$_3$, DMF, NaN$_3$, rt, 4 h, 90%; (c) IM$_4$, CuI, Et$_3$N (anhydrous), 4-bromo-1-butyne, acetonitrile, rt, overnight, under argon, 85%; (d) 4-picolylamine, Pd$_2$(dba)$_3$, xantphos, Cs$_2$CO$_3$, 1,4-dioxane, 100 °C, overnight for L$_1$, 90%; (e) N-Boc-ethylenediamine, Pd$_2$(dba)$_3$, xantphos, Cs$_2$CO$_3$, 1,4-dioxane, 100 °C, overnight,/TFA, DCM, rt, 1.5 h for L3, 80%; (f) 4-picolylamine, 2-picolylamine, Pd$_2$(dba)$_3$, xantphos, Cs$_2$CO$_3$, 1,4-dioxane, 100 °C, overnight for L$_2$ and L$_5$, 88% and 85%, respectively; (g) N-Boc-ethylenediamine, Pd$_2$(dba)$_3$, xantphos, Cs$_2$CO$_3$, 1,4-dioxane, 100 °C, overnight/TFA, DCM, rt, 1.5 h for L$_4$, 80%; (h) IM$_5$, K$_2$CO$_3$, acetone, 60 °C, 10 h for L$_6$ and L$_{10}$, 75% and 78%, respectively; (i) 1,2-dibromoethane, K$_2$CO$_3$, acetone, 60C, 8 h, 90%; (j) IM$_6$, NaN$_3$, DMF, rt, 12 h, 85%; (k) 4-alkynyl-2,2′-bipyridine, CuI, Et$_3$N, acetonitrile, 10 h for L$_7$, 90%; (l) imidazole, Cs$_2$CO$_3$, DMF, 110 °C, overnight for L$_8$, 85%; (m) N-boc-ethylenediamine, DMF(anhydrous), 80 °C, 4−5h/TFA, DCM, rt, 1.5 h for L$_9$, 80%.

structure analysis for ReL$_2$, ReL$_5$ and ReL$_7$ (*vide infra*). As expected infrared spectra of rhenium complexes ReL$_1$-ReL$_{10}$ showed two bands corresponding to the ν(CO) symmetric A1 and asymmetric E stretching modes at ca. 2030 (s) and 1905 (br) cm^{-1}, respectively (see Table 1). ^{1}H NMR spectra in acetonitrile-d3 showed, for *fac*-[Re(CO)$_3$(bpy)L$_\#$]$^+$ complexes, a characteristic low-field shift of the bipyridine protons, indicative of the successful displacement of the triflate ion. In coordinating solvents (acetonitrile-d3, methanol-d4, DMSO-d_6 or a mixture of water and methanol), we found no evidence of ligand displacement or solvent exchange for these species over a three days period.

Complexes ReL$_1$-ReL$_{10}$ show very similar UV−Vis spectra (Table 1). A very pronounced and intense absorption band centered at 330 nm with a shoulder at 310 nm characterize them (Fig. 2). Because coumarins are important fluorophores, widely used in both material and biological sciences due to their inherent physicochemical and photophysical characteristics [68−72], we also investigated the emissive properties of the complexes. Upon excitation at 360 nm all complexes exhibit emission in the blue range of the visible spectrum with emission bands between 420 and 470 nm (Table 1). The only exception is ReL$_1$, which emits green light (528 nm) under the same conditions.

Scheme 2. Synthetic routes of rhenium complexes ReL$_1$-ReL$_{10}$. Conditions: a) bidentate ligands, toluene, reflux, 12 h, under argon, 90−95%; b) 2,2′-bipyridine, toluene, reflux, 12h, under argon, 98%; c) CF$_3$SO$_3$H, DCM, rt, 1 h, 85%; d) monodentate ligands, MeOH, reflux, 12 h, under argon/NH$_4$PF$_6$, MeOH, rt, 0.5−1 h, 95−98%.

Table 1
Photophysical properties of ReL$_1$-ReL$_{10}$.

| Complexes	Absorption λ_{max} [nm][a]	Emission λ_{max} [nm][b]	vCO [cm^{-1}][c]	
			A1	E
ReL$_1$	330, 310 (sh)	528	1905	2028
ReL$_2$	330, 310 (sh)	453	1908	2029
ReL$_3$	331, 312 (sh)	470	1902	2022
ReL$_4$	335, 307 (sh)	460	1897	2023
ReL$_5$	330, 311 (sh)	454	1934	2018
ReL$_6$	340, 309 (sh)	428	1905	2028
ReL$_7$	338, 328 (sh)	424	1922	2017
ReL$_8$	330, 311 (sh)	427	1901	2026
ReL$_9$	338, 310 (sh)	425	1861	2017
ReL$_{10}$	342, 311 (sh)	424	1910	2026

[a] In CH$_3$CN; sh = shoulder.
[b] In CH$_3$CN; λ_{ex} = 360 nm.
[c] In KBr.

2.2. X-ray crystallography

Single crystals suitable for X-ray diffraction analysis for 3-arylcoumarin ligands L$_1$, L$_2$, L$_5$, L$_6$ and L$_8$ were obtained by slow evaporation of a chloroform or acetonitrile solution of the molecules (Fig. 2). Similarly, crystals of ReL$_2$ and ReL$_5$ were grown by slow evaporation of acetonitrile:water (2:1) and dichloromethane solutions, respectively, whilst crystals of ReL$_7$ were obtained by slow diffusion of pentane into a chloroform solution of the complex (Fig. 3). Ligands L$_1$, L$_2$, L$_5$, L$_6$ and L$_8$ crystallized in either triclinic (P-1) or monoclinic (P2$_1$/c) lattices with 2 or 4 crystallographically independent but chemically identical molecules in the asymmetric units respectively. With the exception of L$_2$, better described as L$_2$•CHCl$_3$, no other molecule (i.e. solvents, anion or salts) are present in the asymmetric units of the other species. Bond distances and angles of the 3-arylcoumarin cores are virtually identical
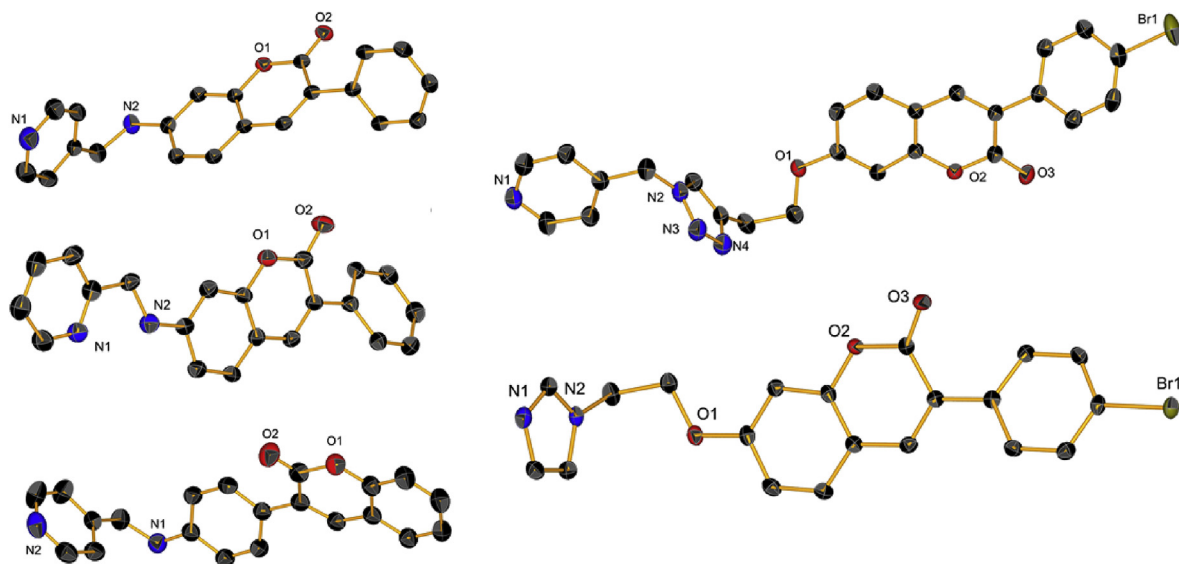
Fig. 2. Ortep representation of left: (from top to bottom) ligands L$_1$, L$_2$, L$_5$, and right: (from top to bottom) L$_6$ and L$_8$. Thermal ellipsoids set at a 30% probability level. Hydrogen atoms, as well as solvent for L$_2$, are omitted for clarity.
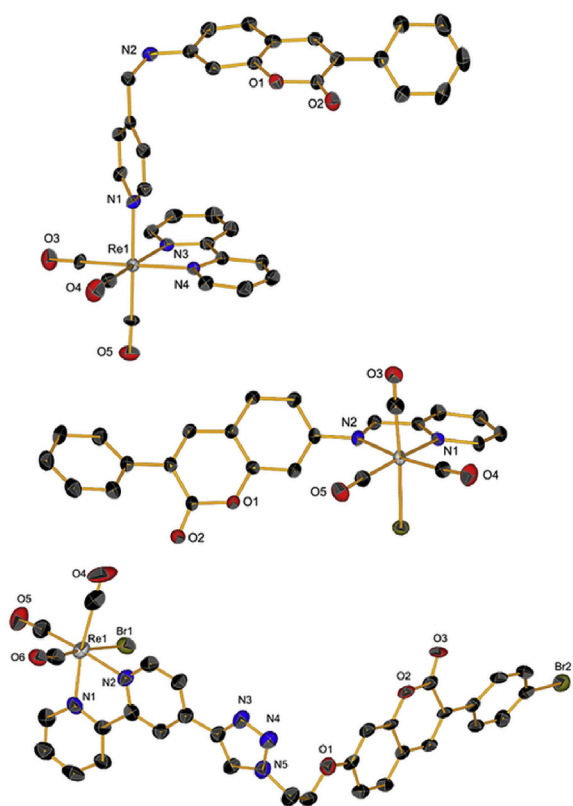
Fig. 3. Ortep representation of (from top to bottom) ReL$_2$, ReL$_5$ and ReL$_7$. Thermal ellipsoids set at a 30% probability level. Hydrogen atoms, as well as solvent and counter ion for ReL$_2$ and minor partitioning for ReL$_5$ and ReL$_7$, are omitted for clarity.

(within 3σ), indicating that the different chemical derivatizations do not affect significantly the electronics of the same.

Rhenium complexes also crystallized in either triclinic (ReL$_5$, P-1) or monoclinic (P2$_1$/c) lattices, again, with 2 or 4 crystallographically independent but chemically identical molecules in the asymmetric units respectively. Ligand to ligand π-stacking interactions dominate

the crystal packing of ReL$_2$ and ReL$_5$, but are absent in ReL$_7$ (ESI). Specifically, coumarin ring to bpy π-stacking is observed in ReL$_2$, interlocking pairs of molecules at a distance of 3.54 Å, while in ReL$_5$ head to tail fully eclipsed coumarin to coumarin ring π-stacking, pairs the two complexes in the asymmetric unit at a distance of 3.68 Å. In ReL$_5$, the carbonyl ligand and the bromide ion *trans* to it are partially disordered, with relative occupancies of 92 and 8%. The exact same disorder is also present in the crystal structure of ReL$_7$ where the ligands show partial occupancies of 87 and 13%. No other molecule are present in the asymmetric units of ReL$_5$ and ReL$_7$, while the PF$_6^-$ counter ion and a molecule of acetonitrile complete the same of ReL$_2$. In all cases, the rhenium ion is in a pseudooctahedral environment in which bond lengths and angles fall within the typical range found for similar tricarbonyl rhenium complexes (CCDC search).

2.3. Antimicrobial and cytotoxic properties

Antimicrobial activity of ReL$_1$-ReL$_{10}$ complexes was determined against Gram-positive bacteria, three *Staphylococcus aureus* strains including methicillin-resistant *S. aureus* (MRSA), *Enterococcus faecium* and *Listeria monocytogenes*, Gram-negative bacterial strain *Pseudomonas aeruginosa*, and four *Candida* spp., including *C. albicans*, *C. glabrata*, *C. krusei* and *C. parapsilosis* (Table 2). In addition, the therapeutic index as a measure of a selective activity against pathogenic microorganism in comparison to the host effect was determined by the zebrafish (*Danio rerio*) model, as a preclinical animal model for toxicity assessment (Table 2). First, the antimicrobial activity of 3-arylcoumarin ligands L$_1$-L$_{10}$ against the same bacteria and fungi was evaluated and minimum inhibitory concentrations (MICs) were determined. With the exception of L$_9$ (MIC = 20 μM against *S. aureus* ATCC 25923 and 10 μM against *Candida* strains) and L$_6$ (MIC = 13 and 25 μM against *C. parapsilosis* and *C. glabrata*, respectively), none of these ligands exhibited activity, with MICs >150 μM (ESI).

Therapeutic Index (**Ti = LC$_{50}$/MIC**) and *Selectivity ind***ex (Si = IC$_{50}$/MIC) are given for the most potent compounds. If is not given the values are ≤ 1.** Therapeutic index for vancomycin was not determined due to its parenteral application and no testing in the zebrafish model. **nd − not determined.** All complexes are

Table 2
Minimum inhibitory concentration (MIC, μg/mL and μM in brackets), therapeutic index (Ti) and selectivity index (Si) of ReL$_1$-ReL$_{10}$ complexes against Gram-positive bacterial and fungal strains.

Complexes	S. aureus ATCC 43300	S. aureus NCTC 6571	S. aureus ATCC 25923	E. faecium ATCC 6057
ReL$_1$	0.7 (0.8)/*16.7/17.5*	0.7 (0.8)/*16.7/17.5*	*2.8 (3.1)/4.2/4.5*	2.8 (3.1)/*4.2/4.5*
ReL$_2$	0.7 (0.8)/*15.7*/4.4	0.7 (0.8)/*15.7*/4.4	*2.8 (3.1)/3.9/1.3*	1.6 (1.8)/*6.9/1.9*
ReL$_3$	7.9 (12.5)/*8/1.1*	7.9 (12.5)/*8/1.1*	**> 500**	>500
ReL$_4$	3.9 (6.2)/*16/1.2*	7.9 (12.5)/*8*	15.8 (25)/*4*	31.5
ReL$_5$	4.2 (6.2)/*16*	4.2 (6.2)/*16*	135.7	135.7
ReL$_6$	0.8 (0.8)/*9.9/26.3*	0.8 (0.8)/*9.9/26.3*	3.3 (3.1)/*2.5/6.8*	1.9 (1.8)/*4.4/11.7*
ReL$_7$	183.7	114.8	**> 500**	>500
ReL$_8$	0.8 (0.8)/*8.5/6*	0.8 (0.8)/*8.5/6*	*1.5 (1.5)/4.4/3*	6.1
ReL$_9$	150.2	187.8	**> 500**	>500
ReL$_{10}$	0.8 (0.8)/*24.2/21.9*	0.8 (0.8)/*24.2/21.9*	3.2 (3.1)/*6.1/5.6*	0.8 (0.8)/*24.3/21.9*
Linezolid	2 (5.9)/*12.5*	2 (5.9)/*12.5*	2 (5.9)/*12.5*	nd
Vancomycin	1(0.7)/nd	2(1.4)/nd	1(0.7)/nd	nd
	C. albicans ATCC 10231	*C. glabrata* ATCC 2001	*C. krusei* ATCC 6258	*C. parapsilosis* ATCC 22019
ReL$_1$	22.5	22.5	11.2/(*1.1*)	22.5
ReL$_2$	11.2	22.5	4.5	11.2
ReL$_3$	>500	>500	>500	>500
ReL$_4$	>500	>500	>500	>500
ReL$_5$	>500	>500	>500	>500
ReL$_6$	13.5/(*1.7*)	13.5/(*1.7*)	13.5/(*1.7*)	<6.7/(>*3.4*)
ReL$_7$	>500	>500	>500	>500
ReL$_8$	4.9	24.6	4.9	4.9
ReL$_9$	>500	>500	>500	>500
ReL$_{10}$	12.9/(*1.4*)	12.9/(*1.4*)	12.9/(*1.4*)	12.9/(*1.4*)

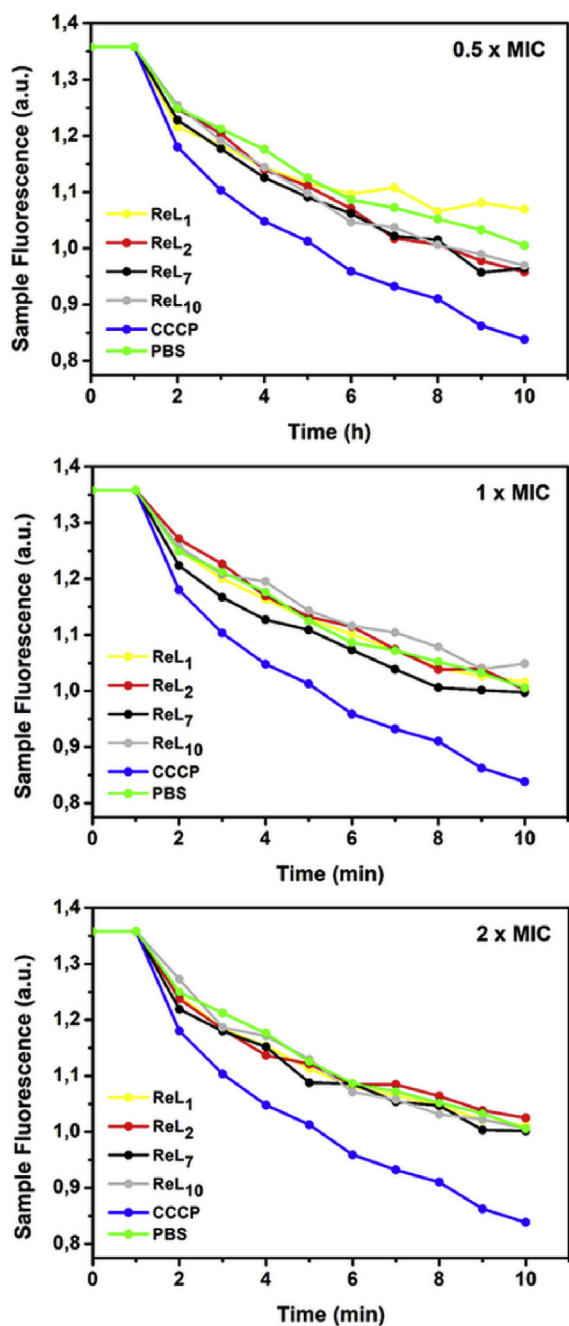inactive against Gram-positive *L. monocytogenes* NCTC 11994 and Gram-negative *P. aeruginosa* PAO1.

On the other hand, all Re complexes showed good activity against Gram-positive bacteria. Among these, complexes ReL$_1$-ReL$_{10}$ exhibited the highest potency against methicillin-resistant *S. aureus* ATCC 43300 (MRSA) and *S. aureus* NCTC 6171, being active in the nanomolar range with MIC values as low as 0.8 μM (700–800 ng/mL). The same species were also active against *E. faecium*, with ReL$_{10}$ exhibiting the highest potency being active at a dose of 0.8 μM (MICs = 800 ng/mL). This finding is particularly interesting, as *S. aureus* and *E. faecum* tend to appear together in hospital infections and usually can survive in nosocomial environments due to an intrinsic resistance to several antibiotics [73–75]. In comparison to other rhenium tricarbonyl antimicrobial species tested against MRSA strains, active ReL# complexes are among the most potent species reported. Their anti-staphylococcal activity is similar to the N-heterocyclic carbene (NHC) *fac*-Re(I)(CO)$_3$ compound containing unsubstituted benzimidazol-2-ylidene and phenanthroline reported by Siegmund et al. [39] and the rhenium bisquinoline complexes of Frei, if photo-activated at 365 nm (1h irradiation) [40].

In addition, it is important to note that the bipyridyl complexes ReL$_1$, ReL$_2$, ReL$_6$, ReL$_8$ and ReL$_{10}$ demonstrated 7.6-fold higher antimicrobial activity against MRSA than linezolid (MIC of 2 μg/mL = 5.9 μM) and comparable effects to vancomycin (MIC of 1 μg/mL = 0.7 μM). These are the antibiotics approved by FDA and recommended by the IDSA guidelines for the treatment of MRSA infections [76]. Vancomycin is the treatment of choice against staphylococcal infections, while linezolid represents the only alternative to vancomycin for the treatment of MRSA-caused nosocomial pneumonia in the USA and Europe, proving to be superior over vancomycin in clinical practice [77]. Together with the [(Cp^{Xbiph})Ir(TolBig)Br]Br complex [24], ReL$_{10}$ is the only other example we know of an organometallic complex showing nanomolar activity against both MRSA and *E. faecum*. Against the Gram-negative *L. monocytogenes* and Gram-negative *P. aeruginosa*, all Re complexes were inactive. Similarly, the complexes exhibit

moderate (ReL$_8$) or low antifungal activity and low selectivity towards tested *Candida* strains (Table 2). Since *S. aureus* is a leading cause of skin and soft tissue infections, in order to examine the rhenium complexes as the potential topical agents, we assessed their cytotoxicity in the model of human lung fibroblasts (MRC-5 cells, Table S2, ESI). According to the ratio between respective IC$_{50}$ and MIC values (Table 2), the complexes ReL$_1$, ReL$_6$ and ReL$_{10}$ showed the best selective index (Si) suggesting their possible application to treat superficial staphylococcal infection.

2.4. S. aureus MRSA membrane potential perturbation and DNA interaction of active complexes

In order to provide initial clues of the possible targets and mechanism of action of active ReL# complexes, we measured *S. aureus* MRSA membrane potential perturbation. The outermost surface of bacterial cells contains negatively charged structures such as teichoic acid and polysaccharide elements embedded in the cytoplasmic membrane of Gram-positive bacteria, or lipopolysaccharide in the outer membrane of Gram-negative bacteria, which are responsible for the initial interaction of the complexes with bacterial cell surface and subsequent uptake [78]. When tested for their potency to disrupt bacterial membrane potential, ReL# complexes did not show any significant effect on *S. aureus* MRSA cell membrane potential, contrary to carbonyl cyanide m-chlorophenyl hydrazone (CCCP), used as positive control (Fig. 4). Next, we investigated DNA interaction with ReL# complexes via gel electrophoresis. Coumarin derivatives are well-known DNA intercalators. Jadoo et al. also reported that Re(I) species of 4-trifluoromethyl coumarin intercalate in the minor groove of Calf-Thymus-DNA [79]. Of all tested complexes only ReL$_1$ and ReL$_2$ significantly interacted with double stranded DNA preventing the interaction of ethidium bromide with lambda bacteriophage DNA (λ-DNA). This indicates that, at least for ReL$_1$ (Fig. 6) and ReL$_2$ (Fig. S32), bacterial DNA might be a target for their mode of action. ReL$_1$, in particular, showed the highest affinity for λ-DNA (Fig. 5).

Fig. 5. *In vitro* interaction of ReL$_1$ with lambda bacteriophage DNA (20 ng/μL, 37 °C, 2 h in 10 mM Tris-Cl, pH 8.5). Concentrations of complex ReL$_1$ are 200, 100, 50, 25, 12.5 and 6.25 μM.

Fig. 4. Measurement of *S. aureus* MRSA cell membrane potential after exposure to different concentrations of selected ReL$_\#$ complexes (from top to bottom: ½ × MIC, 1 × MIC and 2 × MIC). Sample fluorescence refers to that of the 3,3′-diethyloxacarbocyanine iodide (DiOC$_2$(3)) dye and relates to the membrane potential as previously shown [80]. CCCP (carbonyl cyanide 3-chlorophenylhydrazone) can destroy membrane potential by eliminating the proton gradient and was used as a positive control. Data relative to ReL$_1$ were normalized to the fluorescence of the complex in the 1 × MIC and 2 × MIC experiments.

2.5. In vivo toxicity evaluation

To determine whether ReL$_\#$ complexes would be safe for human use, we evaluated their toxic response in the zebrafish model. This is widely used as an animal model for the preclinical toxicity assessment of bioactive molecules, including a variety of metal complexes (e.g. Ag, Au, Pt, Ru, and Ir) [81–83]. Owing to their high genetic, physiological and immunological similarity to humans, and

good correlation in response to pharmaceuticals, zebrafish markedly simplifies the path to clinical trials and reduces failure at later stages of testing [84–86]. To the best of our knowledge, antimicrobial rhenium(I)-tricarbonyl complexes have not been tested for toxicity in animal studies so far, contrary to the anticancer species of the same core, thus making their therapeutic profile against microbial infections largely unknown.

The results of our *in vivo* study showed that ReL$_\#$ complexes with anti-staphylococcal activity are non-toxic at much higher doses of the corresponding MICs against MRSA and *S. aureus* NCTC 6571 (Table 2, Fig. 6A), suggesting their possible application in the treatment of staphylococcal infections. The most active, bipyridyl complexes ReL$_1$, ReL$_2$, ReL$_6$, ReL$_8$ and ReL$_{10}$ appeared more toxic than bidentate complexes ReL$_3$, ReL$_4$, ReL$_5$, ReL$_7$ and ReL$_9$, which correlates with their antimicrobial activity. The latter set of complexes did not provoke any toxic response in zebrafish embryos even at a dose as high as 100 μM. The bipyridyl complexes did not cause teratogenic malformations or cardiovascular side effects (pericardial edema, decreased heart beat rate) in the survived embryos at any tested dose, while after 5-days exposure induced liver toxicity at doses 27-fold higher of the respective MICs against MRSA (≥20 μM). According to the determined LC$_{50}$ values (Table 2), the therapeutic indexes (Ti as the LC$_{50}$ and MIC doses ratio) of antimicrobial ReL$_\#$ complexes ranged from 16 to 24, with the highest Ti value for ReL$_{10}$. Taken together, the data obtained in the zebrafish model indicate that anti-staphylococcal rhenium tricarbonyl complexes could be applied at much higher doses than the effective ones considered *in vitro*, which is of particular significance for microbial strains that may require higher doses for a therapeutic response.

2.6. Antibacterial efficacy in S. aureus-infected zebrafish embryos in vivo system

The antimicrobial efficiency of ReL$_\#$ complexes was evaluated *in vivo* using the zebrafish-*S. aureus* ATCC 43300 infection model. Zebrafish models of infection are widely employed to investigate the pathogenesis of various human-associated microorganisms [87,88] and the differences in virulence between clinical strains [89,90], as well as to discover novel antimicrobials and evaluate their efficacy *in vivo* [81,91,92]. Herein, 30 hpf-old embryos were microinjected with ~1500 bacterial cells into the bloodstream (the circulation valley) to establish systemic infection. Afterward the embryos were exposed to different concentrations of the selected Re complexes, and inspected for their survival over a period of four days post infection (dpi) as a measure of the antimicrobial efficacy. We chose complexes ReL$_1$, ReL$_6$, ReL$_8$, and ReL$_{10}$ as the most potent
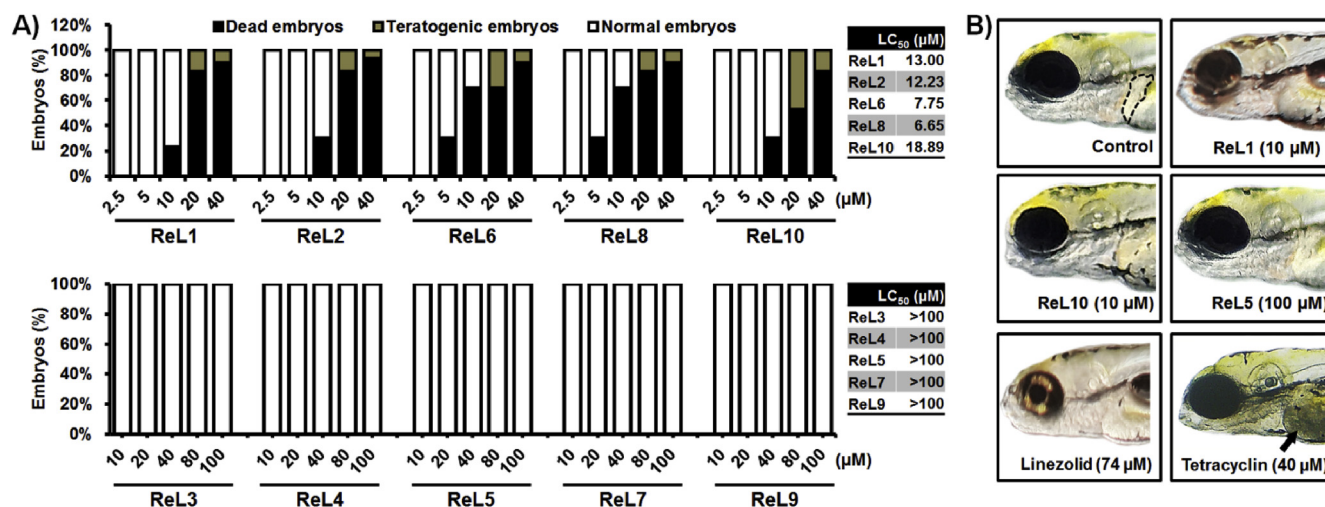
Fig. 6. The *in vivo* toxicity evaluation of complexes ReL$_1$-ReL$_{10}$ in the zebrafish model. Wild type (wt) embryos were treated with different doses of tested complexes at 6 h post fertilization (hpf) and 72 hpf and evaluated for survival, teratogenicity, cardiotoxicity and the hepatotoxicity at 120 hpf, respectively (n = 30 per a dose) (A). Normally developed embryos, without signs of hepato- and cardiotoxicity, after exposure to 10 μM of ReL$_1$ and ReL$_{10}$ (13 × MICs MRSA for both), 100 μM of ReL$_5$ (32 × MIC against MRSA) and linezolid at 74 μM (13 × MIC against MRSA from 72 to 120 hpf are shown (B). The normal (clear) liver in a control embryo is outlined. Tetracycline caused liver necrosis and darkening (arrow).

ones, and ReL$_5$ having the therapeutic index comparable to that of ReL$_1$ and higher than those of ReL$_6$ and ReL$_8$. Their anti-staphylococcal efficacy was compared to that of the antibiotic linezolid.

In the untreated group, the infected embryos showed the first signs of MRSA infection already 24 h after bacterial cells injection. Signs included abscess like structures, necrotic yolk/yolk buddy extension, appearance of pericardial edema, curved body in some cases (Fig. 7B), and embryos progressively died over time reaching the mortality rate of 60% by 4 dpi (Fig. 7A). The infection readouts observed herein are very similar to those reported by Prajsnar [93]. On the other side, treatments with the rhenium complexes successfully rescued infected embryos from lethal staphylococcal infection, but with different efficiency. The antibacterial efficacy of the rhenium complexes was evident already 24 h after application, providing markedly higher fish survival compared to the untreated group (P < 0.01, log-rank test, Fig. 7A) and the absence of necrotic lesions (abscesses) or pericardial edema (Fig. 7B). Moreover, after 4-days treatments, all rhenium complexes except of ReL$_1$ appeared more effective against MRSA infection than linezolid at the same dose (P < 0.05, log-rank test). ReL$_{10}$ appeared to be most potent complex rescuing all infected fish already at ½ × MIC dose, followed by ReL$_5$ which achieved the same protective effect at 1 × MIC and 2 × MIC doses. Out of four tested complexes, ReL$_1$ demonstrated the lowest efficacy against MRSA *in vivo* (active only at ≥ 1 × MIC doses), but again comparable to that of linezolid (P = 0.54 log-rank test), increasing the survival rate of infected fish up to 90% at the highest applied dose.

In order to determine whether the applied complexes also reduced bacterial burden in rescued fish, the fluorescence intensity of infected embryos correlating with bacterial number and the number of viable bacteria (CFU) per embryo was assessed after the 4-days treatment. In comparison to the control, we found that MRSA infection markedly decreased following complexes administration (P < 0.05) according to the fluorescence decline (Fig. 7C) and the CFU reduction up to 2 log (Fig. 7D). Furthermore, no bacteria were recorded in some embryos receiving 2 × MIC dose of ReL$_{10}$ (Fig. 7D), which was significantly more effective than linezolid in MRSA clearance at each of applied dose (P < 0.003).

It is important to note that all rescued fish following ReL$_\#$ treatment developed without adverse toxic effects by 4 dpi (120 hpf), including cardiotoxicity, hepatotoxicity and teratogenicity (not shown). Obtained data regarding anti-MRSA potency *in vivo* are different from *in vitro* data. This is not surprising considering the multicellular complexity of the organism, different conditions and growth rate of bacterial cells within embryos, the contribution of embryonic innate immune cells (neutrophils and macrophages) and infected tissue response in the resolving infection, as well as the metabolic transformation and possible immunomodulatory effect of the absorbed molecules. To the best of our knowledge, there is still lack of *in vivo* data demonstrating the antimicrobial activity for this class of compounds [21]. Our *in vivo* study in the zebrafish model showed that the rhenium complexes may be effective antimicrobial agents, with a particular emphasis against MRSA infection. Our complexes demonstrated better *in vivo* anti-staphylococcal activity than linezolid, being active in the nano-molar range and without toxic side effects at higher dose of the effective MIC.

3. Conclusion

In this study we have reported the synthesis, characterization and antimicrobial properties of a series of 3-arylcoumarin molecules and their respective *fac*-[Re(CO)$_3$(bpy)L]$^+$ and *fac*-[Re(CO)$_3$(L⌒L)Br] complexes. Whereas the organic 3-arylcoumarin ligands are virtually inactive against the pathogens if administered alone, when coordinated to the *fac*-[Re(CO)$_3$]$^+$ core, the bactericidal potency of the resulting complexes is enhanced by 2-3 orders of magnitude. Several of rhenium complexes exhibit potent *in vitro* activity against methicillin-resistant *Staphylococcus aureus* (MRSA)) with minimum inhibitory concentrations (MICs) in the nanomolar range (700−800 ng/mL). However, *in vivo* (zebrafish-*S. aureus* infection model) complexes proved effective in rescuing MRSA-infected embryos at lowers doses (as low as 350 ng/mL). Furthermore, the complexes with anti-staphylococcal/MRSA activity are non-toxic to the embryos, and are able to increase infected fish rate survival up to 100%. All rescued fish following treatment with the complexes developed without adverse toxic effects. The molecules do not affect bacterial cell membrane potential, but some of the most potent complexes strongly interact with DNA, indicating it as a possible target for their mode of action. Nearly all compounds are ineffective against *Candida* fungal strains. Overall,
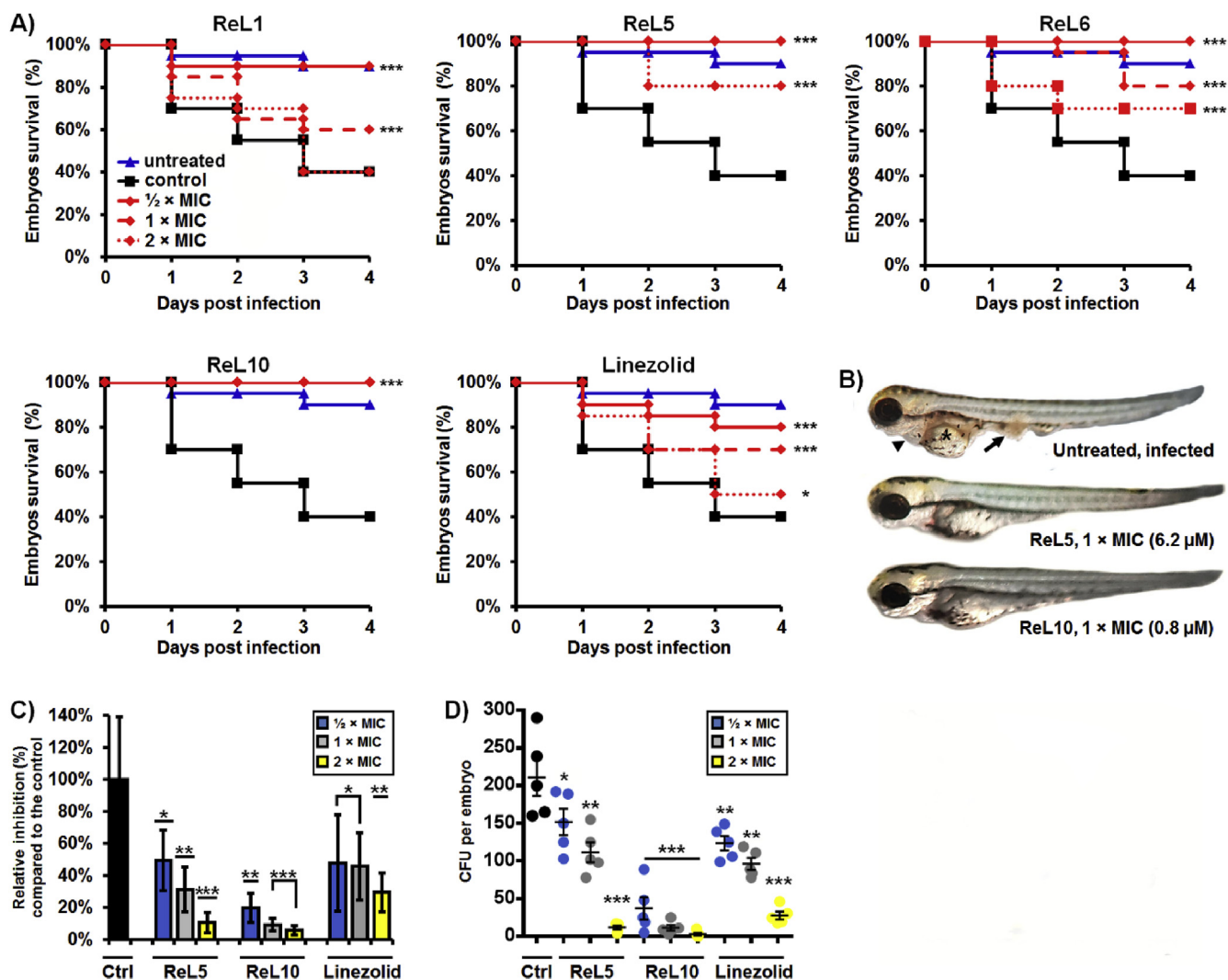
Fig. 7. The tricarbonyl rhenium(I) complexes ReL$_1$, ReL$_5$, ReL$_6$ and ReL$_{10}$ efficiently rescued the zebrafish embryos of the lethal MRSA-infection. Wild type (wt) zebrafish embryos were infected with 1500 cells of *S. aureus* ATCC 43300 into the circulation valley and incubated at 31 °C (n = 30 per dose). The Kaplan-Meier survival curves of the MRSA-infected embryos upon different doses of the selected complexes and linezolid are shown (A). Morphology of infected embryos at 1 dpi without antimicrobial treatment and treated with ReL$_5$ and ReL$_{10}$ are shown (B). Signs of the MRSA infection in untreated embryos were visible already at 24 h after bacterial cells injection, such as the abscess-like structures in yolk buddy extension (arrow), yolk necrosis (asterisk), an appearance of pericardial edema (arrowhead) and curved body. The antimicrobial efficacy of the applied compounds was assessed by monitoring fluorescence of bacterial burden in the whole body (C) and determining CFU per embryos (D) after the 4-days treatment (n = 5−10). Efficacy based on fluorescence data is expressed as a percentage of inhibition of MRSA proliferation relative to the level for DMSO-treated control groups. Data are normalized in relation to the control group and shown as the mean ± SD. Significance in inhibition is indicated with asterisks (*P < 0.05; **P < 0.01; ***P < 0.001).

our data indicate that ReL$_\#$ species could find potential application in antimicrobial therapy against MRSA infections. Future studies will address their *in vivo* antimicrobial efficacy against clinical MRSA isolates from various specimens (e.g. cystic fibrosis, soft tissues, wounds) and decipher their molecular targets and mode of action.

4. Experimental section

Materials and methods. All chemicals were purchased in reagent or analytical grade from commercial suppliers (Sigma-Aldrich, Alfa Aesar, TCI, Fluorochem) and used without further purification. Solvents were either used as received or dried over molecular sieves prior to use. ^{1}H and ^{13}C NMR spectra were recorded on a Bruker Avance III 400 MHz using residual solvent peaks as internal references. The following abbreviations are used: singlet (s), doublet (d), doublet of doublets (dd), triplet (t), doublet of

triplets (td), quintuplet (quint), sextuplet (sext), and multiplet (m). High resolution mass spectrometry was performed on a Bruker FTMS 4.7-T Apex II (BRUKER DALTONICS GmbH, Switzerland). The following abbreviations are used: high-resolution mass spectrometry (HRMS), electrospray ionization (ESI). HPLC analyses were performed on a Merck-Hitachi L7000. The analytical separations were conducted on a Macherey−Nagel Nucleodur PolarTec column (5 μm particle size, 110 Å pore size, 250 × 3 mm). The preparative separations were conducted on a Macherey−Nagel Nucleodur C18 HTec column (5 μm particle size, 110 Å pore size, 250 × 21 mm). The flow rate was set to 0.5 ml/min for analytical separations and 5 ml/min for the preparative ones. The eluting bands were detected at 320 nm. Analytical thin-layer chromatography (TLC) was performed on commercial silica plates (Merck 60-F 254, 0.25 mm thickness); compounds were visualized by UV light (254 nm and 366 nm). Preparative flash chromatography was performed with Merck silica gel (Si 60, 63−200 mesh). IR spectra were recorded on

a PerkinElmer Spectrum 100 FT-IR spectrometer. The UV−Vis spectra were recorded on a Jasco V-730 and the emission on a spectrofluorometer FS5 (Edinburgh Instruments Ltd). Single crystal diffraction collections were done on Stoe IPDS2 diffractometer (MoKα₁ (λ = 0.71073 Å)) equipped with a cryostat from Oxford Cryosystems. The structure were solved with the ShelXT structure solution program [94] using Intrinsic Phasing and refined with the ShelXL refinement package [95] using Least Squares minimisation. All the crystal structures have been deposited at the Cambridge Crystallographic Data Centre. CCDC numbers 1977993−1978000 contain the supplementary crystallographic data for this paper. These data can be obtained free of charge from the Cambridge Crystallographic Data Centre via www.ccdc.cam.ac.uk/structures.

DFT and TDDFT calculations. All computations were performed with the Gaussian 09 programs. Geometry optimizations as well as frequency calculations were performed in the gas phase. The hybrid meta-GGA functional wB97XD [96−100], designed to account for dispersion, was used in combination with the standard SDD basis sets [101]. For the spin state of the complexes (singlet state in all cases), the default spin formalism was followed in the calculations and default Gaussian 09 values were adopted for the numerical integration grids, self-consistent-field (SCF) and geometry optimization convergence criteria. Geometries were optimized without symmetry restrictions. The nature of the stationary points was checked by computing vibrational frequencies in order to verify true minima. No negative frequencies were observed for the reported values. Electronic transition energies and oscillator strengths were then calculated at their wB97XD -optimized geometries using TDDFT. For these calculations the 25 lowest energy electronic excitations were calculated for each compound, and solvent effects were added via a solvent continuum dielectric model using acetonitrile as the solvent. The calculated molecular orbitals were visualized using GaussView.

4.1. Synthesis and characterization of compounds L₁-L₁₀

General procedure for the synthesis of 3-arylcoumarins. 7-bromo-3-phenyl-2H-chromen-2-one (IM₁), 3-(4-bromophenyl)-2H-chromen-2-one (IM₂) and 3-(4-bromophenyl)-7-hydroxy-2H-chromen-2-one (IM₃). All glassware used for the preparation of 3-arylcoumarins was prepared to 300 °C and reactions were performed in anhydrous conditions. To a solution of 4-bromo-phenyl-acetic acid (1.0 equiv.) and the corresponding salicylaldehyde (1.0 equiv.) in Ac₂O (anhydrous), CH₃CO₂K (1.8 equiv.) was added at room temperature (rt) under argon, and the mixture was heated to reflux overnight. After it had cooled to rt, the reaction mixture was neutralized by using 20% aqueous NaHCO₃. Ethyl acetate was added to the aqueous phase and the organic layer was extracted (3 ×). The combined organic layers were washed with distilled water and brine, dried with anhydrous Na₂SO₄ and finally evaporated under reduced pressure. The crude compound was recrystallized from ethanol giving the acetoxylated intermediate. IM₁, IM₂, IM₃ were prepared by the hydrolysis of their acetoxylated counterparts with 2 N aqueous HCl in MeOH and the reaction mixture was refluxed for 3−4h. Then the solution was cooled to rt, and kept in an ice-bath for 20min. The solid product was filtered and washed with cold distilled water (3 ×), and dried under vacuum. The desired 3-arylcoumarin intermediates were obtained in 90−95% of yield (no further purification was necessary).

General procedure for the synthesis of L₁, L₂, L₅. To a solution of IM₁ or IM₂ (1.0 equiv.) in 1,4-dioxane under argon, Pd₂(dba)₃ (0.05 equiv), xantphos (0.1 equiv.) and Cs₂CO₃ (1.5 equiv.) were added and the mixture stirred at rt for 5 min. Picolylamine (1.8 equiv.) was then added and the reaction mixture degassed for 15 min. The temperature was increased to 100 °C and stirred

overnight. After completion of the reaction, the solvent was evaporated, the residue was dissolved in DCM and the solution was filtered. Then the filtrate was loaded on silica gel for purification by normal phase column chromatography. The desired product eluted at 50:50 EtOAc:pentane. The organic layer was concentrated at reduced pressure to yield the product.

3-(4-((2-aminoethyl)amino)phenyl)-2H-chromen-2-one (L₁). Yellow solid, yield 90%, ESI-MS(m/z) calcd. for C₂₁H₁₆N₂O₂ 328.12, found 328.0 [M + H]⁺. ¹H NMR (400 MHz, DMSO-d₆) δ 8.51 (d, J = 5.62 Hz, 2H), 8.06 (s, 1H), 7.72 (d, J = 1.47 Hz, 1H), 7.50−7.57 (m, 3H), 7.33 (d, J = 0.98 Hz, 4H), 6.75 (s, 1H), 6.63 (d, J = 5.01 Hz, 2H), 4.39 (d, J = 6.24 Hz, 2H). ¹³C NMR (101 MHz, chloroform-d) δ 161.0, 153.1, 149.9, 148.8, 148.0, 137.3, 130.7, 129.7, 128.1, 127.5, 124.4, 124.3, 122.1, 120.0, 116.3, 112.6, 77.4, 77.2, 77.0, 76.7, 46.8.

3-phenyl-7-((pyridin-4-ylmethyl)amino)-2H-chromen-2-one (L₂). Yellow solid, yield 88%, ESI-MS(m/z) calcd. for C₂₁H₁₆N₂O₂ 328.12, found 328.0 [M + H]⁺. ¹H NMR (400 MHz, chloroform-d) δ 8.46−8.55 (m, 2H), 7.55−7.65 (m, 3H), 7.31−7.36 (m, 2H), 7.25−7.30 (m, 1H), 7.18−7.24 (m, 3H), 6.47 (dd, J = 2.26, 8.50 Hz, 1H), 6.38 (d, J = 2.20 Hz, 1H), 4.90 (t, J = 5.81 Hz, 1H), 4.39 (d, J = 5.87 Hz, 2H). ¹³C NMR (101 MHz, chloroform-d) δ 161.3, 155.9, 150.6, 150.0, 147.7, 140.4, 135.4, 129.1, 128.4, 128.3, 128.1, 122.7, 122.0, 111.2, 110.9, 98.3, 77.3, 77.2, 77.0, 76.7, 46.6.

3-phenyl-7-((pyridin-2-ylmethyl)amino)-2H-chromen-2-one (L₅). Yellow solid, yield 85%, ESI-MS(m/z) calcd. for C₂₁H₁₆N₂O₂ 328.12, found 328.0 [M + H]⁺. ¹H NMR (400 MHz, chloroform-d) δ 8.61−8.66 (m, 1H), 7.68−7.74 (m, 4H), 7.41−7.47 (m, 2H), 7.35−7.39 (m, 2H), 7.31−7.34 (m, 1H), 7.25−7.28 (m, 1H), 6.67 (dd, J = 2.26, 8.50 Hz, 1H), 6.56 (d, J = 2.20 Hz, 1H), 5.68 (br. s., 1H), 4.54 (s, 2H). ¹³C NMR (101 MHz, chloroform-d) δ 171.1, 161.5, 156.5, 156.1, 151.1, 149.2, 140.7, 136.9, 135.6, 128.9, 128.3, 128.3, 127.9, 122.5, 121.9, 121.8, 111.3, 110.7, 97.9, 60.4, 48.3.

General procedure for the synthesis of L₃, L₄. To the solution of IM₁ or IM₂ (1.0 equiv.) in 1,4-dioxane under argon, Pd₂(dba)₃ (0.05 equiv.), xantphos (0.1 equiv.) and Cs₂CO₃ (1.5 equiv.) were added and the mixture stirred at rt for 5 min. Boc-N-ethylendiemine (1.8 equiv.) was then added and the reaction mixture was degassed for 15 min. The temperature was increased to 100 °C and stirred overnight. After completion of the reaction, the solvent was evaporated, the residue was dissolved in DCM and the solution was filtered. Then the filtrate was loaded on silica gel for purification by normal phase column chromatography. The desired product eluted at 1:6 EtOAc:pentane. The organic layer was concentrated at reduced pressure to yield the N-boc intermediates. To prepare L₃ and L₄, (1.0 equiv.) of the N-Boc-protected intermediate was reacted with TFA in CH₂Cl₂ and stirred at rt for 1.5h. The residue was dissolved in DCM and carefully neutralized by saturated 20% NaHCO₃. The organic layer was then washed with water followed by brine. The organic layer was concentrated. The crude product was purified by recrystallization in DCM to yield pure L₃ and L₄.

3-(4-((2-aminoethyl)amino)phenyl)-2H-chromen-2-one (L₃). Yellow solid, yield 80%, ESI-MS(m/z) calcd. for C₁₇H₁₆N₂O₂ 280.33, found 281.1 [M + H]⁺. ¹H NMR (400 MHz, methanol-d₄) δ 7.95 (s, 1H), 7.67 (dd, J = 1.53, 7.64 Hz, 1H), 7.50−7.62 (m, 3H), 7.31−7.38 (m, 2H), 6.69−6.76 (m, 2H), 3.28 (s, 1H), 3.23−3.30 (m, 2H), 2.84−2.92 (m, 2H), 2.13−2.15 (m, 1H). ¹³C NMR (101 MHz, methanol-d₄) δ 161.5, 152.8, 149.5, 137.1, 130.3, 129.2, 129.2, 127.8, 127.6, 126.9, 124.3, 122.6, 120.3, 115.5, 111.8, 111.8, 45.3, 40.2.

7-((2-aminoethyl)amino)-3-phenyl-2H-chromen-2-one (L₄). Yellow solid, yield 85%, ESI-MS(m/z) calcd. for C₁₇H₁₆N₂O₂ 280.33, found 281.1 [M + H]⁺. ¹H NMR (400 MHz, methanol-d₄) δ 7.82 (s, 1H), 7.57−7.58 (m, 1H), 7.55 (s, 1H), 7.28−7.36 (m, 3H), 7.23−7.27 (m, 1H), 6.60 (dd, J = 2.26, 8.62 Hz, 1H), 6.48 (d, J = 2.08 Hz, 1H), 3.42 (t, J = 6.17 Hz, 2H), 3.07 (t, J = 6.17 Hz, 2H), ¹³C NMR (101 MHz, methanol-d₄) δ 162.1, 156.0, 151.9, 141.5, 135.5, 129.2, 128.0, 128.0,

127.9, 127.9, 127.5, 121.1, 111.3, 110.6, 96.6, 40.2, 38.2.

General procedure for preparation of 4-((4-(2-bromoethyl)-1H-1,2,3-triazol-1-yl)methyl)pyridine (IM5). 4-(Bromomethyl) pyridine hydrobromide (1.0 equiv.) was dissolved in DMF. Potassium carbonate (1.0 equiv.) was added to the mixture and stirred for 15 min. Sodium azide (1.5 equiv.) was added to the reaction mixture and it stirred at rt for 4h. Afterward, DCM and cold water were added to the mixture and two phases were separated (3 ×). The combined organic layers were washed with brine and water, dried over Na_2SO_4 and then filtered. The solvent was evaporated under reduced pressure giving 4-(azidomethyl)pyridine (85%), as a yellowish oily residue, which was used for the next step without further purification. To a solution of 4-(azidomethyl)pyridine (1.0 equiv.) in acetonitrile (dry), CuI (0.1 equiv.) and Et_3N (0.4 equiv., anhydrous) were added at rt and the solution stirred for 5 min under argon. 4-bromo-1-butyne (1.05 equiv.) was then added and the reaction stirred under argon at rt for 12 h, after which time a mixture of ice, brine and DCM was added. The two phases were separated, the organic layers were collected, washed with water twice, combined, washed with brine and finally dried over sodium sulfate and filtered. The solvent was evaporated under reduced pressure leaving a greenish residue which was loaded on silica for flash column chromatography. The desired product eluted at 100:1 EtOAc:MeOH. The pure product (IM5) was obtained as a yellow liquid (90%).

General procedure for preparation of L6, L10. To a solution of IM3 (1.0 equiv.) in acetone, potassium carbonate (8.0 equiv) was added and the solution stirred at rt for 10 min. Then, IM5 (1.0 equiv.) was added to the mixture and heated to reflux (60 °C) for 10h. Then, the mixture was filtered and the solvent evaporated. The residue was purified using flash column chromatography. The desired product eluted at 9:1 EtOAc:pentane. L6 and L10 were obtained (75%) and (78%), respectively.

3-(4-bromophenyl)-7-(2-(1-(pyridin-4-ylmethyl)-1H-1,2,3-triazol-4-yl)ethoxy)-2H-chromen-2-one (L6). White solid, yield 75%, ESI-MS(m/z) calcd. for $C_{25}H_{19}BrN_4O_3$ 503.35, found 503.0. ^1H NMR (400 MHz, chloroform-d) δ 8.59–8.69 (m, 2H), 7.77 (s, 1H), 7.55–7.62 (m, 4H), 7.40–7.50 (m, 2H), 7.04–7.18 (m, 2H), 6.78–6.92 (m, 2H), 5.57 (s, 2H), 4.37 (t, J = 6.42 Hz, 2H), 3.30 (d, J = 12.84 Hz, 2H), ^{13}C NMR (101 MHz, chloroform-d) δ 161.8, 160.5, 155.3, 150.6, 144.9, 143.6, 139.9, 133.8, 131.6, 130.0, 129.1, 123.9, 122.8, 122.2, 122.1, 113.4, 112.9, 101.3, 67.3, 52.7, 25.9.

3-(4-chlorophenyl)-7-(2-(1-(pyridin-4-ylmethyl)-1H-1,2,3-triazol-4-yl)ethoxy)-2H-chromen-2-one (L10). White-yellowish solid, yield 78%, ESI-MS(m/z) calcd. for $C_{25}H_{19}ClN_4O_3$ 458.90, found 459.0. ^1H NMR (400 MHz, chloroform-d) δ 8.49–8.57 (m, 2H), 7.67 (s, 1H), 7.54 (br. s., 2H), 7.39 (s, 1H), 7.29–7.36 (m, 3H), 6.97–7.07 (m, 2H), 6.72–6.80 (m, 2H), 5.46 (br. s., 2H), 4.27 (t, J = 6.42 Hz, 2H), 3.20 (t, J = 6.42 Hz, 2H). ^{13}C NMR (101 MHz, chloroform-d) δ 161.8, 160.5, 155.3, 150.6, 144.9, 143.6, 139.9, 133.8, 133.5, 130.0, 129.1, 128.6, 123.9, 122.1, 113.4, 112.9, 101.3, 67.3, 52.7, 25.9.

General procedure for preparation of 7-(2-bromoethoxy)-3-(4-bromophenyl)-2H-chromen-2-one (IM6). To a solution of IM3 (1.0 equiv.) in acetone, potassium carbonate (2.0 equiv.) was added and the mixture stirred for 5 min under argon. Then 1,2-dibromoethane (7.0 equiv.) was added to the solution dropwise in 10 min. The mixture was heated to 60 °C and stirred overnight. After completion of the reaction, the solution was filtered and washed with acetone (2 ×). The filtrate was concentrated under reduced pressure and the residue was recrystallized in acetonitrile to yield the pure product IM6 (90%).

7-(2-(4-([2,2′-bipyridin]-4-yl)-1H-1,2,3-triazol-1-yl)ethoxy)-3-(4-bromophenyl)-2H-chromen-2-one (L7). To a solution of IM6 (1.0 equiv.) in DMF under argon, NaN_3 (1.5 equiv.) was added and

stirred at rt for 4–5 h. The mixture was added to cold brine, then EtOAc was used to extract the crude product (3 ×) from the aqueous phase. The organic layers were collected and concentrated by reduced pressure. The oily brown residue was purified by a normal phase column chromatography. The desired product eluted at 60:40 EtOAc:pentane and 7-(2-azidoethoxy)-3-(4-bromophenyl)-2H-chromen-2-one (IM7) was obtained (95%) as a white solid. The final step to synthesize L7 was a click reaction, to a solution of IM7 (1.0 equiv.) in acetonitrile. CuI (0.1 equiv.), Et_3N (anhydrous, 0.4 equiv.) and 4-ethynyl-2,2′-bipyridine (1.0 equiv.) were added and then the mixture was stirred for 12 h at rt. After the completion of the reaction, the solvent was evaporated and the crude product was purified by flash column chromatography. The product eluted at 99:1 EtOAc:MeOH and yielded to L7 (90%). White solid, yield 90%, ESI-MS(m/z) calcd. for $C_{29}H_{20}BrN_5O_3$ 566.42, found 566.0. ^1H NMR (400 MHz, DMSO-d_6) δ 9.06 (s, 1H), 8.86 (d, J = 2.45 Hz, 1H), 8.70–8.79 (m, 2H), 8.38–8.46 (m, 1H), 8.25 (s, 1H), 7.98 (dt, J = 1.77, 7.73 Hz, 1H), 7.87–7.93 (m, 1H), 7.60–7.74 (m, 5H), 7.43–7.56 (m, 1H), 7.08–7.17 (m, 1H), 6.96–7.06 (m, 1H), 4.93 (t, J = 5.01 Hz, 2H), 4.66 (d, J = 10.03 Hz, 2H). ^{13}C NMR (101 MHz, DMSO-d_6): δ (ppm) 161.48, 160.14, 156.63, 155.45, 155.22, 150.67, 150.59, 149.76, 144.73, 141.46, 139.47, 137.85, 134.53, 131.61, 130.84, 130.38, 124.89, 124.67, 122.74, 122.01, 121.06, 120.26, 116.47, 113.86, 113.62, 101.57, 67.11, 49.74.

7-(2-(1H-imidazol-1-yl)ethoxy)-3-(4-bromophenyl)-2H-chromen-2-one (L8). To a solution of IM6 (1.0 equiv.) in DMF (anhydrous), imidazole (1.5 eqiuv.) and cesium carbonate (2.0 equiv.) were added. The solution was heated to 110 °C and stirred overnight. After the completion of the reaction, the mixture was added to cold brine, then EtOAc was used to extract the crude product (3 ×) from the aqueous phase. The organic layers were collected and concentrated by reduced pressure giving an oily brown residue. The crude product was purified by flash column chromatography. The product eluted at EtOAc and resulted in L8. White solid, yield 90%, ESI-MS(m/z) calcd. for $C_{20}H_{15}BrN_2O_3$ 411.26, found 410.9. ^1H NMR (400 MHz, acetonitrile-d_3) δ 7.99 (s, 1H), 7.61–7.67 (m, 4H), 7.56–7.60 (m, 2H), 7.16 (t, J = 1.22 Hz, 1H), 6.96 (t, J = 0.98 Hz, 1H), 6.92–6.95 (m, 2H), 4.39–4.43 (m, 2H), 4.35–4.38 (m, 2H). ^{13}C NMR (101 MHz, acetonitrile-d_3) δ 161.6, 160.3, 155.4, 140.7, 137.8, 134.7, 131.4, 130.4, 129.7, 128.8, 123.5, 122.0, 119.7, 117.4, 113.8, 113.0, 101.2, 68.1, 49.0, 45.9.

7-(2-((2-aminoethyl)amino)ethoxy)-3-(4-bromophenyl)-2H-chromen-2-one (L9). To a solution of IM6 (1.0 equiv.) in DMF, N-Boc-ethylenediimine (1.2 equiv.) was added. The mixture was then heated to 80 °C and stirred overnight. After the reaction completion, the N-protected intermediate (1.0 equiv.) was dissolved in DCM (dry) and stirred at rt, then TFA (3.0 equiv.) was added to the mixture which was stirred at rt for 1.5h. The residue was dissolved in dichloromethane and carefully neutralized by saturated 20% $NaHCO_3$. The organic layer was washed with brine followed by water and then concentrated. The crude product was purified by flash chromatography. The product eluted at 97:3 DCM:NH_4OH in MeOH 5% giving L9. White solid, yield 80%, ESI-MS(m/z) calcd. for $C_{20}H_{15}BrN_2O_3$ 403.28, found 403.0. ^1H NMR (400 MHz, methanol-d_4) δ 7.88 (s, 1H), 7.49–7.53 (m, 2H), 7.43–7.48 (m, 3H), 6.86 (dd, J = 2.38, 8.62 Hz, 1H), 6.81 (d, J = 2.20 Hz, 1H), 5.40 (s, 1H), 4.08 (t, J = 5.26 Hz, 4H), 3.22 (td, J = 1.65, 3.30 Hz, 1H), 3.18–3.25 (m, 1H), 3.16–3.28 (m, 3H), 2.90–2.97 (m, 2H), 2.90–2.98 (m, 2H), 2.75–2.79 (m, 2H), 2.70–2.79 (m, 3H), 2.69–2.75 (m, 2H). ^{13}C NMR (101 MHz, acetone-d_6) δ 161.5, 159.7, 155.4, 140.5, 134.6, 131.2, 130.4, 129.7, 123.2, 121.8, 113.8, 113.2, 101.1, 66.6, 56.1, 53.2, 42.9.

Preparation of fac-[Re(CO)3(bpy)L#]PF6 complexes. To a solution of [BrRe(CO)5] (1.0 equiv.) in hot toluene, bipyridine (1.0 equiv.) was added and refluxed for 7–9h. After it had cooled to the room temperature, the reaction mixture was filtered and washed

with cold toluene (2 ×), yielding *fac*-[Re(CO)$_3$(bpy)Br] as yellow powder. The complex was suspended in DCM under argon and trifluoromethanesulfonic acid was added and the mixture stirred for 30 min at rt. *fac*-[Re(CO)$_3$(bpy)(CF$_3$SO$_3$)], as a green-yellowish solid, was precipitated by slow addition of diethyl ether. To a solution of *fac*-[Re(CO)$_3$(bpy)(CF$_3$SO$_3$)] in MeOH, the monodentate ligand was added and mixture heated to 65 °**C**. The reaction was refluxed under argon for 10h. To obtain the final products, NH$_4$PF$_6$ (6.0 equiv) was added to the solution. After precipitation of the final complex, the mixture was filtered and washed with water to remove the excess NH$_4$PF$_6$.

fac-**[Re(CO)$_3$(bpy)L$_1$]PF$_6$ (ReL$_1$)**. Yellow solid, yield 95%, ESI-MS(*m/z*) calcd. for C$_{34}$H$_{24}$N$_4$O$_5$Re$^+$ (M$^+$) 754.80, found 754.90. IR (solid, νCO cm^{-1}): 2028, 1905 ^{1}H NMR (400 MHz, acetonitrile-d$_3$) δ 9.22 (dd, *J* = 0.73, 5.50 Hz, 2H), 8.39–8.43 (m, 2H), 8.28 (dd, *J* = 1.47, 15.89 Hz, 2H), 8.14–8.18 (m, 2H), 7.85–7.89 (m, 1H), 7.78 (d, *J* = 1.22 Hz, 2H), 7.62–7.66 (m, 1H), 7.53–7.59 (m, 1H), 7.49 (d, *J* = 4.77 Hz, 2H), 7.33 (d, *J* = 1.10 Hz, 2H), 7.28–7.30 (m, 2H), 6.53 (d, *J* = 4.77 Hz, 2H), 5.40 (t, *J* = 6.24 Hz, 1H), 4.38 (d, *J* = 6.24 Hz, 2H). ^{13}C NMR (101 MHz, acetonitrile-d$_3$) δ 195.5, 160.7, 155.9, 155.1, 153.9, 153.1, 152.9, 151.7, 148.1, 141.2, 137.4, 130.8, 129.8, 129.7, 128.9, 128.0, 127.8, 124.9, 124.8, 124.8, 124.5, 123.9, 121.4, 120.3, 115.9, 112.2, 45.3.

fac-**[Re(CO)$_3$(bpy)L$_2$]PF$_6$ (ReL$_2$)**. Yellow solid, yield 95%, ESI-MS(*m/z*) calcd. for C$_{34}$H$_{24}$N$_4$O$_5$Re$^+$ (M$^+$) 754.80, found 754.90. IR (solid, νCO cm^{-1}): 2029, 1908 ^{1}H NMR (400 MHz, acetonitrile-d$_3$) δ 9.22 (dd, *J* = 0.61, 5.50 Hz, 2H), 8.39 (s, 2H), 8.25–8.31 (m, 2H), 8.15–8.19 (m, 2H), 7.85–7.87 (m, 1H), 7.77–7.82 (m, 2H), 7.66–7.70 (m, 2H), 7.42–7.47 (m, 2H), 7.35–7.41 (m, 2H), 7.27 (s, 2H), 6.58 (d, *J* = 2.20 Hz, 1H), 6.20–6.22 (m, 1H), 5.88 (s, 1H), 4.42 (d, *J* = 6.36 Hz, 2H). ^{13}C NMR (101 MHz, acetonitrile-d$_3$) δ 195.9, 160.9, 156.0, 155.9, 153.9, 151.9, 151.2, 141.2, 140.9, 136.0, 129.4, 128.9, 128.4, 128.3, 127.9, 124.9, 124.8, 121.6, 111.4, 110.6, 97.1, 45.11.

fac-**[Re(CO)$_3$(bpy)L$_6$]PF$_6$ (ReL$_6$)**. Pale yellow solid, yield 95%, ESI-MS(*m/z*) calcd. for C$_{38}$H$_{27}$BrN$_6$O$_6$Re$^+$ (M$^+$) 929.78, found 928.9. IR (solid, νCO cm^{-1}): 2029, 1906 ^{1}H NMR (400 MHz, acetonitrile-d$_3$) δ 9.00 (dd, *J* = 0.79, 5.44 Hz, 2H), 8.45 (br. s., 2H), 8.36 (d, *J* = 8.19 Hz, 2H), 8.16–8.24 (m, 2H), 8.01 (s, 1H), 7.93 (s, 1H), 7.65–7.70 (m, 3H), 7.54–7.63 (m, 3H), 6.90–6.97 (m, 2H), 6.67 (d, *J* = 4.77 Hz, 2H), 5.14 (s, 2H), 4.36 (t, *J* = 5.99 Hz, 2H), 3.41 (t, *J* = 5.93 Hz, 2H). ^{13}C NMR (101 MHz, acetonitrile-d$_3$) δ 195.9, 161.6, 160.4, 156.6, 155.3, 153.9, 149.9, 148.6, 142.8, 140.8, 140.7, 134.6, 131.4, 130.4, 129.8, 127.8, 125.9, 124.0, 123.5, 122.6, 122.0, 113.8, 113.0, 101.3, 66.1, 53.4, 27.1.

fac-**[Re(CO)$_3$(bpy)L$_8$]PF$_6$ (ReL$_8$)**. Yellow solid, yield 95%, ESI-MS(*m/z*) calcd. for C$_{33}$H$_{23}$BrN$_4$O$_6$Re$^+$ (M$^+$) 837.68, found 836.9. IR (solid, νCO cm^{-1}): 2026, 1901 ^{1}H NMR (400 MHz, acetonitrile-d$_3$) δ 9.16 (dd, *J* = 0.73, 5.50 Hz, 2H), 8.39 (d, *J* = 8.19 Hz, 2H), 8.24 (dt, *J* = 1.53, 7.92 Hz, 2H), 8.02 (s, 1H), 7.73 (ddd, *J* = 1.22, 5.56, 7.64 Hz, 2H), 7.66 (d, *J* = 1.83 Hz, 4H), 7.59 (d, *J* = 9.29 Hz, 1H), 7.46–7.54 (m, 1H), 7.50 (d, *J* = 24.58 Hz, 1H), 7.46–7.52 (m, 1H), 7.07 (t, *J* = 1.47 Hz, 1H), 6.71–6.76 (m, 2H), 6.57 (t, *J* = 1.47 Hz, 1H), 4.25 (d, *J* = 4.89 Hz, 2H), 4.21 (d, *J* = 4.89 Hz, 2H). ^{13}C NMR (101 MHz, acetonitrile-d$_3$) δ 195.9, 161.3, 160.6, 156.0, 155.4, 154.0, 141.2, 140.9, 140.7, 134.8, 131.7, 130.6, 130.0, 129.1, 128.8, 124.8, 123.9, 122.4, 122.3, 117.6, 114.2, 113.0, 101.4, 47.4.

fac-**[Re(CO)$_3$(bpy)L$_{10}$]PF$_6$ (ReL$_{10}$)**. Pale yellow solid, yield 95%, ESI-MS(*m/z*) calcd. for C$_{37}$H$_{27}$ClN$_7$O$_6$Re$^+$ (M$^+$) 885.33, found 884.9. IR (solid, νCO cm^{-1}): 2026, 1910, 1892 ^{1}H NMR (400 MHz, acetonitrile-d$_3$) δ 9.00 (d, *J* = 5.50 Hz, 2H), 8.51 (br. s., 2H), 8.36 (d, *J* = 8.19 Hz, 2H), 8.20 (dt, *J* = 1.34, 7.95 Hz, 2H), 7.91–8.04 (m, 2H), 7.68–7.77 (m, 2H), 7.56–7.65 (m, 3H), 7.45–7.53 (m, 2H), 6.88–6.97 (m, 2H), 6.71 (br. s., 2H), 5.15 (s, 2H), 4.36 (t, *J* = 6.05 Hz, 2H), 3.41 (t, *J* = 5.99 Hz, 2H). ^{13}C NMR (101 MHz, acetonitrile-d$_3$) δ 195.9, 161.6, 160.4, 156.6, 155.3, 153.9, 149.9, 148.6, 142.8, 140.8, 140.7, 134.6, 131.4, 130.4, 129.8, 127.8, 125.9, 124.0, 123.5, 122.6, 122.0, 113.8, 113.0, 101.3, 66.1, 53.4, 27.1.

Preparation of *fac*-[Re(CO)$_3$(L$_#$)Br] complexes. Bromopentacarbonylrhenium(I) (1.0 equiv.) was dissolved in hot toluene (110 °C) under argon. The diimine ligand (1.0 equiv.) was added, and the solution was refluxed overnight. The mixture was cooled to room temperature, and if a precipitate had formed, it was isolated by centrifugation, washed with cold toluene and cold diethyl ether, and dried in vacuo. Otherwise, the solvent was evaporated, and the crude compound was chromatographed by flash chromatography on silica gel using ethyl DCM/MeOH (100:3, v/v) as eluent to give the pure products described below.

fac-**[Re(CO)$_3$(L$_3$)Br] (ReL$_3$)**. Light brown solid, yield 95%, ESI-MS(*m/z*) calcd. for C$_{20}$H$_{16}$BrN$_2$O$_5$Re (M-Br)$^+$ 550.56, found 550.8. IR (solid, νCO cm^{-1}): 2023, 1902, 1876 ^{1}H NMR (400 MHz, acetone-d$_6$) δ 8.08 (s, 1H), 7.73–7.78 (m, 2H), 7.64–7.68 (m, 1H), 7.47–7.52 (m, 1H), 7.24–7.28 (m, 4H), 5.86–5.87 (m, 1H), 5.07 (d, *J* = 5.14 Hz, 1H), 3.94 (d, *J* = 7.70 Hz, 1H), 3.37–3.48 (m, 3H), 3.13–3.26 (m, 1H). ^{13}C NMR (101 MHz, acetone-d$_6$) δ 159.7, 153.6, 149.5, 139.9, 132.1, 131.5, 129.4, 128.5, 126.7, 124.5, 119.9, 119.1, 115.9, 53.8, 42.9.

fac-**[Re(CO)$_3$(L$_4$)Br] (ReL$_4$)**. Dark cream solid, yield 93%, ESI-MS(*m/z*) calcd. for C$_{20}$H$_{16}$BrN$_2$O$_5$Re (M-Br)$^+$ 550.56, found 550.8. IR (solid, νCO cm^{-1}): 2023, 1897 ^{1}H NMR (400 MHz, acetone-d$_6$) δ 8.16 (s, 2H), 7.82–7.85 (m, 2H), 7.80–7.82 (m, 2H), 7.78–7.80 (m, 2H), 7.50 (t, *J* = 1.77 Hz, 1H), 7.47–7.48 (m, 2H), 7.46–7.47 (m, 2H), 7.44–7.45 (m, 1H), 7.42–7.44 (m, 1H), 7.31–7.34 (m, 4H), 6.21–6.28 (m, 2H), 5.27 (d, *J* = 5.26 Hz, 2H), 4.07–4.15 (m, 2H), 3.62–3.67 (m, 4H), 3.59 (dt, *J* = 3.06, 6.05 Hz, 2H), 3.32–3.43 (m, 2H). ^{13}C NMR (101 MHz, acetone-d$_6$) δ 159.5, 154.1, 152.2, 139.6, 135.2, 129.2, 128.6, 128.5, 128.2, 126.9, 117.1, 116.6, 105.9, 53.3, 43.0.

fac-**[Re(CO)$_3$(L$_5$)Br] (ReL$_5$)**. Brown-reddish solid, yield 90%, ESI-MS(*m/z*) calcd. for C$_{24}$H$_{15}$BrN$_2$O$_5$Re (M-Br)$^+$ 597.60, found 598.9. IR (solid, νCO cm^{-1}): 2018, 1934 ^{1}H NMR (400 MHz, acetone-d$_6$) δ 8.77 (d, *J* = 5.26 Hz, 1H), 8.01–8.11 (m, 2H), 7.78–7.84 (m, 1H), 7.70–7.76 (m, 1H), 7.65 (d, *J* = 1.22 Hz, 2H), 7.49 (br. s., 1H), 7.33–7.34 (m, 1H), 7.29–7.32 (m, 2H), 7.25–7.29 (m, 2H), 7.03 (br. s., 1H), 5.10–5.27 (m, 2H). ^{13}C NMR (101 MHz, acetone-d$_6$) δ 162.1, 159.9, 153.0, 151.9, 140.0, 139.5, 135.1, 131.7, 129.7, 129.0, 128.6, 128.2, 127.1, 125.5, 122.9, 116.3, 106.0, 103.9, 59.0.

fac-**[Re(CO)$_3$(L$_7$)Br] (ReL$_7$)**. Yellow solid, yield 95%, ESI-MS(*m/z*) calcd. for C$_{32}$H$_{20}$Br$_2$N$_5$O$_6$Re (M-Br)$^+$ 836.65, found 835.8. IR (solid, νCO cm^{-1}): 2018, 1922, 1889 ^{1}H NMR (400 MHz, DMSO-d$_6$) δ 9.20 (s, 1H), 9.11 (d, *J* = 1.10 Hz, 1H), 9.06 (d, *J* = 5.87 Hz, 2H), 8.91 (d, *J* = 8.19 Hz, 1H), 8.39 (dt, *J* = 1.41, 7.92 Hz, 1H), 8.25 (s, 1H), 8.20 (dd, *J* = 1.59, 5.87 Hz, 1H), 7.75–7.83 (m, 1H), 7.61–7.73 (m, 5H), 7.14 (d, *J* = 2.20 Hz, 1H), 7.02 (dd, *J* = 2.45, 8.68 Hz, 1H), 5.01 (t, *J* = 4.65 Hz, 2H), 4.65 (t, *J* = 4.77 Hz, 2H). ^{13}C NMR (101 MHz, DMSO-d$_6$) δ 161.4, 160.1, 156.5, 155.6, 155.2, 154.2, 153.6, 143.2, 141.8, 141.4, 140.7, 134.5, 131.6, 130.8, 130.4, 128.5, 126.6, 125.0, 123.0, 122.8, 122.0, 120.2, 113.9, 113.6, 101.6, 67.3, 50.0.

fac-**[Re(CO)$_3$(L$_9$)Br] (ReL$_9$)**. Cream-yellowish solid, yield 90%, ESI-MS(*m/z*) calcd. for C$_{22}$H$_{17}$Br$_2$N$_2$O$_6$Re (M) 751.40, found 749.90. IR (solid, νCO cm^{-1}): 2017, 1898, 1862 ^{1}H NMR (400 MHz, acetone-d$_6$) δ 8.15 (s, 1H), 7.75 (s, 1H), 7.70 (d, *J* = 8.44 Hz, 1H), 7.62 (s, 2H), 7.01–7.07 (m, 2H), 5.05 (d, *J* = 3.42 Hz, 1H), 4.57–4.66 (m, 1H), 4.47–4.56 (m, 1H), 4.13 (br. s., 1H), 3.84–3.92 (m, 1H), 3.73–3.83 (m, 1H), 3.52–3.68 (m, 2H), 3.17–3.32 (m, 2H), 2.78–2.89 (m, 2H). ^{13}C NMR (101 MHz, methanol-d$_4$) δ 162.3, 160.8, 155.1, 140.8, 134.1, 131.0, 131.0, 129.9, 129.9, 129.4, 122.7, 121.9, 113.4, 113.0, 100.5, 67.7, 53.4, 49.7, 39.9.

Antimicrobial assays. The minimum inhibitory concentrations (MICs) against a panel of bacteria and *Candida* spp. (all obtained from the National Collection of Type Cultures (NCTC) and the American Type Culture Collection (ATCC)) were determined according to the standard broth microdilution assays, recommended by CLSI (Clinical and Laboratory Standards Institute. Methods for Dilution Antimicrobial Susceptibility Tests for Bacteria That Grow

Aerobically; Approved Standard - Tenth Edition M07-A10. CLSI) and EUCAST (European Committee on Antimicrobial Susceptibility Testing, EUCAST antifungal MIC method for yeasts, v 7.3.1), respectively. The test strains studied were cultured in Luria-Bertani broth (Biolife Italiana S.r.l., Milano, Italy) and RPMI 1640 medium (Gibco) and diluted to give the concentration of 5×10^5 CFU/mL for bacterial and 1×10^5 CFU/mL for fungal cells, respectively. The complexes in liquid broth were serially diluted in the sterile 96-well plate to give the volume of 100 μL. The media solutions with microorganisms were then dispensed to each well to make the final volume of 200 μL, and the final concentration of complexes was in the range 0.125−800 μM. All the plates were covered and incubated at 37 °C for 18 h without shaking. Inhibition of bacterial growth was determined measuring absorbance at 600 nm (OD600), using a Tecan Infinite 200 Pro multiplate reader (Tecan Group Ltd., Männedorf, Switzerland). The negative control (media only) and positive control (only microorganisms in liquid broth) on the same plate were used as references to determine the growth inhibition of bacteria. Samples with inhibition values above 90% were classified as active agents.

In vitro cytotoxicity. *In vitro* cytotoxicity was determined as antiproliferative activity by (3-(4,5-dimethylthiazol-2-yl)-2,5-diphenyltetrazolium bromide (MTT) assay [102] on human lung fibroblasts (MRC-5) obtained from American Type Culture Collection (ATCC) collection. The cells, cultured in the complete RPMI 1640 medium (Merck, Munich, Germany) as a monolayer ($1 \cdot 10^4$ cells per well), were incubated with test compounds at concentrations ranging from 3.1 to 100 μM, in humidified atmosphere of 95% air and 5% CO_2 at 37 °C and the cell viability was measured after 48 h. The extent of MTT reduction was measured spectrophotometrically at 540 nm using Tecan Infinite 200 Pro multiplate reader (Tecan Group Ltd., Männedorf, Switzerland) and the cell survival was expressed as percentage of the control (DMSO treated cells) arbitrarily set to 100%. Cytotoxicity is expressed as the concentration of the compound inhibiting growth by 50% (IC_{50}).

S. aureus membrane perturbation assessment. The depolarization of plasma membrane potential of *S. aureus* ATCC43300 MRSA was determined as described previously by using the membrane potential-sensitive fluorescent dye $DiOC_2(3)$ (3,3′-Diethyloxacarbocyanine Iodide) [80]. Briefly, *S. aureus* MRSA was grown to the early exponential phase (OD_{625nm} of 0.3) in LB, washed with PBS (pH 7.4) and resuspended in PBS containing 1% (w/v) glucose (10^8 colony-forming units of bacteria per mL). Bacteria were incubated at 37 °C for 15 min, followed by incubation with 3 μM $DiOC_2(3)$ under the same conditions (37 °C for 15 min). After the incubation period bacteria were transferred to 96 well plate (100 μl per well) and treated with different compounds. Carbonyl cyanide m-chlorophenyl hydrazone (CCCP, 0.25 μM) was used as positive control (at final concentration of 0.025 μM). The fluorescence change (excitation 485 nm, emission 630 nm) was measured immediately after the addition of compounds on a Tecan Infinite 200 Pro multiplate reader (Tecan Group Ltd., Mannedorf, Switzerland).

DNA interaction *via* gel electrophoresis. DNA interaction assay using gel electrophoresis was conducted according to the previously published procedure [103] using commercial lambda bacteriophage DNA (300 ng, Thermo Scientific™). DNA solution of the final concentration 20 ng/μL was incubated with 400 μM, 200 μM, 100 μM of ReL# compounds (in addition, lower concentrations of ReL1 of 50 μM, 25 μM, 12.5 μM, 6.25 μM were used) in 15 μL reaction volume. After 1 h incubation at 37 °C, samples were mixed with loading dye and analysed via gel electrophoresis (300 ng DNA per lane, 0.8% agarose gel) with ethidium bromide (EthBr) against a HyperLadder™ 1 kb DNA Ladder plus (FastGene) at 60 V for 1 h. Gels were visualized and analysed using the Gel Doc EZ system

(Bio-Rad, Life Sciences, Hercules, USA), equipped with the Image Lab™ Software.

In vivo toxicity. Toxicity evaluation of Re(I)-tricarbonyl complexes was carried in the zebrafish (*Danio rerio*) model according to the general rules of the OECD Guidelines for the Testing of Chemicals (OECD, 2013, Test No. 236) [104]. All experiments involving zebrafish were performed in compliance with the European directive 2010/63/EU and the ethical guidelines of the Guide for Care and Use of Laboratory Animals of the Institute of Molecular Genetics and Genetic Engineering, University of Belgrade. Wild type (AB) zebrafish were kindly provided by dr Ana Cvejić (Wellcome Trust Sanger Institute, Cambridge, UK), raised to adult stage in a temperature- and light-controlled zebrafish facility at 28 °C and standard 14:10-h light-dark photoperiod, and regularly fed with commercially dry flake food (TetraMin™ flakes; Tetra Melle, Germany) twice a day and *Artemia nauplii* once daily. Embryos were produced by pair-wise mating, collected and distributed into 24-well plates containing 10 embryos per well and 1 mL embryos water (0.2 g/L of Instant Ocean® Salt in distilled water) and raised at 28 °C. For assessing lethality, developmental toxicity and cardiotoxicity, the embryos staged at 6 h post fertilization (hpf) were exposed to different concentrations of the tested compounds, and inspected for apical endpoints (Table S1) every day by 120 hpf upon an inverted microscope (CKX41; Olympus, Tokyo, Japan). Linezolid was used as a reference anti-staphylococcal antibiotic. DMSO (0.25%) was used as negative control. Dead embryos were counted and discarded every 24 h. Experiments were performed two times using 30 embryos per concentration. At 120 hpf, embryos were inspected for heartbeat rate, anesthetized by addition of 0.1% (w/v) tricaine solution (Sigma-Aldrich, St. Louis, MO), photographed and killed by freezing at −20 °C for ≥24 h. In addition to developmental and cardio-toxicity, Re(I)tricarbonyl complexes were evaluated for hepatotoxicity. Wild types embryos were exposed to non-lethal doses of the rhenium complexes in a period from 72 hpf (a stage when liver is perfused with blood and a metabolically active) to 120 hpf, and inspected for the hepatotoxicity endpoints (the liver necrosis and darkening, the yolk necrosis and reduced consumption) as previously described by He et al. [105]. Tetracycline-hydrochloride was used as a hepatotoxic antibiotic (positive control) [105]. The experiment was performed two times using 20 embryos per a concentration.

Testing of anti-MRSA efficacy *in vivo*. To address antimicrobial efficacy of rhenium complexes, wild type zebrafish embryos were challenged to *S. aureus* ATCC 43300 infections, according to the protocol previously described by Prajsnar [88]. Bacteria used to infect embryos were grown overnight in Brain-heart infusion (BHI) broth, diluted at 1:100 ration and incubated at 37 °C to reach a mid of exponential phase. After centrifugation (4500 × *g*, 10 min), bacterial pellet was washed three times in PBS and adjusted to OD_{600} (optical density at 600 nm) of 3×10^8 cells/mL. Bacterial cells were than labelled with 2 μM CellTracker™ RedCMTPX (Thermofisher Scientific) according to the manufacturer's instructions. Prior infection, embryos were manually dechorionated at 24 hpf stage and keep at 28 °C. At 30 hpf, anesthetized embryos were microinjected with 5 nL containing ~1500 labelled MRSA cells into the circulation valley by a pneumatic picopump (PV820, World Precision Instruments, USA) aimed to establish fast systemic infection. To confirm bacterial numbers in each injection, a few infected embryos was crashed immediately and the viable counts was determined on solid BHI agar plates after incubation for 4 days at 37 °C. After injection, embryos were incubated to recover for 2 h at 31 °C, dead embryos were removed, and alive embryos were transferred into 24-well plates containing 1 mL of embryo water and 10 embryos per well. The infected embryos were treated with three doses (½ × MIC, 1 × MIC and 2 × MIC) of the selected

complex, and maintained at 31 °C by 120 hpf. Linezolid was used as a positive control. Twenty embryos were used per concentration. Embryos injected with PBS and treated with 0.25% DMSO were used as a control group. The survival and development of infected embryos was recorded every day until 120 hpf (corresponding to fourth days post infection). To evaluate antimicrobial efficacy, bacterial infection was quantified in survived embryos at 4 dpi by monitoring the fluorescence intensity of whole embryos correlating with bacterial burden and determining the number of viable bacteria (CFU - colony forming unit) per embryo [88,92]. Fluorescence was determined at ex./em. wave lengths of 577/602 (spectral characteristics of the fluorescent CellTracker™ Red CMTPX probe) using a Tecan Infinite 200 Pro multiplate reader (Tecan Group Ltd., Männedorf, Switzerland). To determine CFU per embryo, five embryos per each group was manually crushed and plated in BHI agar medium. CFU was determined after incubation at 37 °C for a few days.

Statistical analysis. Survival experiments were evaluated using the Kaplan−Meier method. Comparisons between curves were made using the log rank test. Analysis was performed using GraphPad Prism version 6.0 and statistical significance was assumed at P-value below 0.05.

Declaration of competing interest

The authors declare that they have no known competing financial interests or personal relationships that could have appeared to influence the work reported in this paper.

Acknowledgement

Appendix A. Supplementary data

Supplementary data to this article can be found online at https://doi.org/10.1016/j.ejmech.2020.112533.

References

[1] M.A. Brockhurst, F. Harrison, J.W. Veening, E. Harrison, G. Blackwell, Z. Iqbal, C. Maclean, Assessing evolutionary risks of resistance for new antimicrobial therapies, Nat. Ecol. Evol. 3 (2019) 515−517.

[2] V. Cattoir, B. Felden, Future antibacterial strategies: from basic concepts to clinical challenges, J. Infect. Dis. 220 (2019) 350−360.

[3] S. Cascioferro, B. Parrino, D. Carbone, D. Schillaci, E. Giovannetti, G. Cirrincione, P. Diana, Thiazoles, their benzofused systems, and thiazolidinone derivatives: versatile and promising tools to combat antibiotic resistance, J. Med. Chem. (2020). https://pubs.acs.org/doi/10.1021/acs.jmedchem.9b01245. In press.

[4] M.E.A. de Kraker, A.J. Stewardson, S. Harbarth, Will 10 million people die a year due to antimicrobial resistance by 2050? PLoS Med. 13 (2016) e1002184-e1002184.

[5] R.J. Fair, Y. Tor, Antibiotics and bacterial resistance in the 21st century, Perspect. Med. Chem. 6 (2014) 25−64.

[6] V.L. Simpkin, M.J. Renwick, R. Kelly, E. Mossialos, Incentivising innovation in antibiotic drug discovery and development: progress, challenges and next steps, J. Antibiot. 70 (2017) 1087−1096.

[7] C. Kallberg, C. Ardal, H. Salvesen Blix, E. Klein, E.M. Martinez, M. Lindbaek, K. Outterson, J.A. Rottingen, R. Laxminarayan, Introduction and geographic availability of new antibiotics approved between 1999 and 2014, PloS One 13 (2018), e0205166.

[8] N.G. Simoes, A.F. Bettencourt, N. Monge, I.A.C. Ribeiro, Novel antibacterial agents: an emergent need to win the battle against infections, Mini Rev. Med. Chem. 17 (2017) 1364−1376.

[9] Q. Hu, H. Cheng, W. Yuan, F. Zeng, W. Shang, D. Tang, W. Xue, J. Fu, R. Zhou, J. Zhu, J. Yang, Z. Hu, J. Yuan, X. Zhang, Q. Rao, S. Li, Z. Chen, X. Hu, X. Wu, X. Rao, Panton-Valentine leukocidin (PVL)-positive health care-associated methicillin-resistant *Staphylococcus aureus* isolates are associated with skin and soft tissue infections and colonized mainly by infective PVL-encoding

[10] bacteriophages, J. Clin. Microbiol. 53 (2015) 67−72.

[10] N.D. Friedman, K.S. Kaye, J.E. Stout, S.A. McGarry, S.L. Trivette, J.P. Briggs, W. Lamm, C. Clark, J. MacFarquhar, A.L. Walton, L.B. Reller, D.J. Sexton, Health care–associated bloodstream infections in adults: a reason to change the accepted definition of community-acquired infections, Ann. Intern. Med. 137 (2002) 791−797.

[11] J.S. Francis, M.C. Doherty, U. Lopatin, C.P. Johnston, G. Sinha, T. Ross, M. Cai, N.N. Hansel, T. Perl, J.R. Ticehurst, K. Carroll, D.L. Thomas, E. Nuermberger, J.G. Bartlett, Severe community-onset pneumonia in healthy adults caused by methicillin-resistant *Staphylococcus aureus* carrying the Panton-Valentine leukocidin genes, Clin. Infect. Dis. 40 (2005) 100−107.

[12] S.S. Lewis, V.J. Walker, M.S. Lee, L. Chen, R.W. Moehring, C.E. Cox, D.J. Sexton, D.J. Anderson, Epidemiology of methicillin-resistant *Staphylococcus aureus* pneumonia in community hospitals, Infect. Control Hosp. Epidemiol. 35 (2014) 1452−1457.

[13] A.P. Kourtis, K. Hatfield, J. Baggs, Y. Mu, I. See, E. Epson, J. Nadle, M.A. Kainer, G. Dumyati, S. Petit, S.M. Ray, M.a.g. Emerging Infections Program, D. Ham, C. Capers, H. Ewing, N. Coffin, L.C. McDonald, J. Jernigan, D. Cardo, Vital signs: epidemiology and recent trends in methicillin-resistant and in methicillin-susceptible *Staphylococcus aureus* bloodstream infections - United States, MMWR Morb. Mortal. Wkly. Rep. 68 (2019) 214−219.

[14] A. Hassoun, P.K. Linden, B. Friedman, Incidence, prevalence, and management of MRSA bacteremia across patient populations—a review of recent developments in MRSA management and treatment, Crit. Care 21 (2017) 211.

[15] F.C. Tenover, S.W. Sinner, R.E. Segal, V. Huang, S.S. Alexandre, J.E. McGowan, M.P. Weinstein, Characterisation of a *Staphylococcus aureus* strain with progressive loss of susceptibility to vancomycin and daptomycin during therapy, Int. J. Antimicrob. Agents 33 (2009) 564−568.

[16] M. Patra, G. Gasser, N. Metzler-Nolte, Small organometallic compounds as antibacterial agents, Dalton Trans. 41 (2012) 6350−6358.

[17] L. Szczupak, A. Kowalczyk, D. Trzybinski, K. Wozniak, G. Mendoza, M. Arruebo, D. Steverding, P. Staczek, K. Kowalski, Organometallic ciprofloxacin conjugates with dual action: synthesis, characterization, and antimicrobial and cytotoxicity studies, Dalton Trans. 49 (2020) 1403−1415.

[18] F. Li, J.G. Collins, F.R. Keene, Ruthenium complexes as antimicrobial agents, Chem. Soc. Rev. 44 (2015) 2529−2542.

[19] K.D. Mjos, C. Orvig, Metallodrugs in medicinal inorganic chemistry, Chem. Rev. 114 (2014) 4540−4563.

[20] A. Frei, J. Zuegg, A.G. Elliott, M. Baker, S. Braese, C. Brown, F. Chen, G.D. C, G. Dujardin, N. Jung, A.P. King, A.M. Mansour, M. Massi, J. Moat, H.A. Mohamed, A.K. Renfrew, P.J. Rutledge, P.J. Sadler, M.H. Todd, C.E. Willans, J.J. Wilson, M.A. Cooper, M.A.T. Blaskovich, Metal complexes as a promising source for new antibiotics, Chem. Sci. 11 (2020) 2627−2639.

[21] A. Frei, Metal complexes, an untapped source of antibiotic potential? Antibiotics (2020) 9.

[22] N. Jain, P. Alam, I.R. Laskar, J. Panwar, 'Aggregation induced phosphorescence' active iridium(iii) complexes for integrated sensing and inhibition of bacterial growth in aqueous solution, RSC Adv. 5 (2015) 61983−61988.

[23] P.V. Simpson, C. Schmidt, I. Ott, H. Bruhn, U. Schatzschneider, Synthesis, cellular uptake and biological activity against pathogenic microorganisms and cancer cells of rhodium and iridium *N*-heterocyclic carbene complexes bearing charged substituents, Eur. J. Inorg. Chem. (2013) 5547−5554, 2013.

[24] F. Chen, J. Moat, D. McFeely, G. Clarkson, I.J. Hands-Portman, J.P. Furner-Pardoe, F. Harrison, C.G. Dowson, P.J. Sadler, Biguanide iridium(III) complexes with potent antimicrobial activity, J. Med. Chem. 61 (2018) 7330−7344.

[25] E.M. Lewandowski, J. Skiba, N.J. Torelli, A. Rajnisz, J. Solecka, K. Kowalski, Y. Chen, Antibacterial properties and atomic resolution X-ray complex crystal structure of a ruthenocene conjugated beta-lactam antibiotic, Chem. Commun. 51 (2015) 6186−6189.

[26] A. Frei, R. Rubbiani, S. Tubafard, O. Blacque, P. Anstaett, A. Felgentrager, T. Maisch, L. Spiccia, G. Gasser, Synthesis, characterization, and biological evaluation of new Ru(II) polypyridyl photosensitizers for photodynamic therapy, J. Med. Chem. 57 (2014) 7280−7292.

[27] K.L. Smitten, H.M. Southam, J.B. de la Serna, M.R. Gill, P.J. Jarman, C.G.W. Smythe, R.K. Poole, J.A. Thomas, Using nanoscopy to probe the biological activity of antimicrobial leads that display potent activity against pathogenic, multidrug resistant, gram-negative bacteria, ACS Nano 13 (2019) 5133−5146.

[28] Y. Feng, W.Z. Sun, X.S. Wang, Q.X. Zhou, Selective photoinactivation of methicillin-resistant *Staphylococcus aureus* by highly positively charged Ru(II) complexes, Chem. Eur J. 25 (2019) 13879−13884.

[29] F. Li, J.G. Collins, F.R. Keene, Ruthenium complexes as antimicrobial agents, Chem. Soc. Rev. 44 (2015) 2529−2542.

[30] J. Betts, C. Nagel, U. Schatzschneider, R. Poole, R.M. La Ragione, Antimicrobial activity of carbon monoxide-releasing molecule [Mn(CO)₃(tpa-k³N)]Br versus multidrug-resistant isolates of Avian Pathogenic *Escherichia coli* and its synergy with colistin, PloS One 12 (2017), e0186359.

[31] P. Guntzel, C. Nagel, J. Weigelt, J.W. Betts, C.A. Pattrick, H.M. Southam, R.M. La Ragione, R.K. Poole, U. Schatzschneider, Biological activity of manganese(i) tricarbonyl complexes on multidrug-resistant Gram-negative bacteria: from functional studies to *in vivo* activity in Galleria mellonella, Metallomics 11 (2019) 2033−2042.

[32] P.V. Simpson, C. Nagel, H. Bruhn, U. Schatzschneider, Antibacterial and

antiparasitic activity of manganese(I) tricarbonyl complexes with ketoconazole, miconazole, and clotrimazole ligands, Organometallics 34 (2015) 3809–3815.

[33] R. Olar, M. Badea, D. Marinescu, M.C. Chifiriuc, C. Bleotu, M.N. Grecu, E.E. Iorgulescu, V. Lazar, N,N-dimethylbiguanide complexes displaying low cytotoxicity as potential large spectrum antimicrobial agents, Eur. J. Med. Chem. 45 (2010) 3027–3034.

[34] B.D. Glisic, M.I. Djuran, Gold complexes as antimicrobial agents: an overview of different biological activities in relation to the oxidation state of the gold ion and the ligand structure, Dalton Trans. 43 (2014) 5950–5969.

[35] A. Noor, G.S. Huff, S.V. Kumar, J.E.M. Lewis, B.M. Paterson, C. Schieber, P.S. Donnelly, H.J.L. Brooks, K.C. Gordon, S.C. Moratti, J.D. Crowley, [Re(CO)$_3$]$^+$ complexes of exo-functionalized tridentate "click" macrocycles: synthesis, stability, photophysical properties, bioconjugation, and antibacterial activity, Organometallics 33 (2014) 7031–7043.

[36] M. Wenzel, M. Patra, C.H. Senges, I. Ott, J.J. Stepanek, A. Pinto, P. Prochnow, C. Vuong, S. Langklotz, N. Metzler-Nolte, J.E. Bandow, Analysis of the mechanism of action of potent antibacterial hetero-tri-organometallic compounds: a structurally new class of antibiotics, ACS Chem. Biol. 8 (2013) 1442–1450.

[37] M. Patra, M. Wenzel, P. Prochnow, V. Pierroz, G. Gasser, J.E. Bandow, N. Metzler-Nolte, An organometallic structure-activity relationship study reveals the essential role of a Re(CO)$_3$ moiety in the activity against gram-positive pathogens including MRSA, Chem. Sci. 6 (2015) 214–224.

[38] S.V. Kumar, W.K.C. Lo, H.J.L. Brooks, L.R. Hanton, J.D. Crowley, Antimicrobial properties of mono- and di-fac-rhenium tricarbonyl 2-Pyridyl-1,2,3-triazole complexes, Aust. J. Chem. 69 (2016) 489–498.

[39] D. Siegmund, N. Lorenz, Y. Gothe, C. Spies, B. Geissler, P. Prochnow, P. Nuernberger, J.E. Bandow, N. Metzler-Nolte, Benzannulated Re(i)-NHC complexes: synthesis, photophysical properties and antimicrobial activity, Dalton Trans. 46 (2017) 15269–15279.

[40] A. Frei, M. Amado, M.A. Cooper, M.A.T. Blaskovich, Light-activated rhenium complexes with dual mode of action against bacteria, Chem. Eur J. 26 (2020) 2852–2858.

[41] R.G. Miller, M. Vazquez-Hernandez, P. Prochnow, J.E. Bandow, N. Metzler-Nolte, A CuAAC click approach for the introduction of bidentate metal complexes to a sulfanilamide-derived antibiotic fragment, Inorg. Chem. 58 (2019) 9404–9413.

[42] M.B. Pisano, A. Kumar, R. Medda, G. Gatto, R. Pal, A. Fais, B. Era, S. Cosentino, E. Uriarte, L. Santana, F. Pintus, M.J. Matos, Antibacterial activity and molecular docking studies of a selected series of hydroxy-3-arylcoumarins, Molecules 24 (2019).

[43] J.B. Veselinović, A.M. Veselinović, G.M. Nikolić, S.Z. Pešić, D.B. Stojanović, J.S. Matejić, T.M. Mihajilov-Krstev, Antibacterial potential of selected 4-phenyl hydroxycoumarins: integrated in vitro and molecular docking studies, Med. Chem. Res. 24 (2015) 1626–1634.

[44] J. Sun, W.-X. Ding, X.-P. Hong, K.-Y. Zhang, Y. Zou, Synthesis and antimicrobial activities of 4-aryl-3,4-dihydrocoumarins and 4-arylcoumarins, Chem. Nat. Compd. 48 (2012) 16–22.

[45] M.J. Matos, S. Vazquez-Rodriguez, L. Santana, E. Uriarte, C. Fuentes-Edfuf, Y. Santos, A. Munoz-Crego, Synthesis and structure-activity relationships of novel amino/nitro substituted 3-arylcoumarins as antibacterial agents, Molecules 18 (2013) 1394–1404.

[46] M. Joao Matos, S. Vazquez-Rodriguez, L. Santana, E. Uriarte, C. Fuentes-Edfuf, Y. Santos, A. Munoz-Crego, Looking for new targets: simple coumarins as antibacterial agents, Med. Chem. 8 (2014) 1140–1145.

[47] Z.N. Siddiqui, M.M. N, A. Ahmad, A.U. Khan, Synthesis of 4-hydroxycoumarin heteroarylhybrids as potential antimicrobial agents, Arch. Pharm. 344 (2011) 394–401.

[48] H. Singh, J.V. Singh, K. Bhagat, H.K. Gulati, M. Sanduja, N. Kumar, N. Kinarivala, S. Sharma, Rational approaches, design strategies, structure activity relationship and mechanistic insights for therapeutic coumarin hybrids, Bioorg. Med. Chem. 27 (2019) 3477–3510.

[49] T. Khan, K. Sankhe, V. Suvarna, A. Sherje, K. Patel, B. Dravyakar, DNA gyrase inhibitors: progress and synthesis of potent compounds as antibacterial agents, Biomed. Pharmacother. 103 (2018) 923–938.

[50] A.V. Chate, A.A. Redlawar, G.M. Bondle, A.P. Sarkate, S.V. Tiwari, D.K. Lokwani, A new efficient domino approach for the synthesis of coumarin-pyrazolines as antimicrobial agents targeting bacterial d-alanine-d-alanine ligase, New J. Chem. 43 (2019) 9002–9011.

[51] J.-Y. Yang, J.-H. Park, M.-J. Lee, J.-H. Lee, H.-S. Lee, Antimicrobial effects of 7,8-dihydroxy-6-methoxycoumarin and 7-hydroxy-6-methoxycoumarin analogues against foodborne pathogens and the antimicrobial mechanisms associated with membrane permeability, J. Food Protect. 80 (2017) 1784–1790.

[52] B. Thati, A. Noble, R. Rowan, B.S. Creaven, M. Walsh, M. McCann, D. Egan, K. Kavanagh, Mechanism of action of coumarin and silver(I)–coumarin complexes against the pathogenic yeast Candida albicans, Toxicol. Vitro 21 (2007) 801–808.

[53] O.E. Dahl, New oral antithrombotics: focus on dabigatran, an oral, reversible direct thrombin inhibitor for the prevention and treatment of venous and arterial thromboembolic disorders, Vasc. Health Risk Manag. 8 (2012) 45–57.

[54] F.J.A. Penning-Van Beest, J. Koerselman, R.M.C. Herings, Risk of major bleeding during concomitant use of antibiotic drugs and coumarin anticoagulants, J. Thromb. Haemostasis 6 (2008) 284–290.

[55] C. Kontogiorgis, D. Hadjipavlou-Litina, Biological evaluation of several coumarin derivatives designed as possible anti-inflammatory/antioxidant agents, J. Enzym. Inhib. Med. Chem. 18 (2003) 63–69.

[56] Z.-Q. Liu, W. Yu, Z.-L. Liu, Antioxidative and prooxidative effects of coumarin derivatives on free radical initiated and photosensitized peroxidation of human low-density lipoprotein, Chem. Phys. Lipids 103 (1999) 125–135.

[57] G. Roma, M. Di Braccio, G. Grossi, D. Piras, G. Leoncini, D. Bruzzese, M.G. Signorello, P. Fossa, L. Mosti, Synthesis and in vitro antiplatelet activity of new 4-(1-piperazinyl)coumarin derivatives. Human platelet phosphodiesterase 3 inhibitory properties of the two most effective compounds described and molecular modeling study on their interactions with phosphodiesterase 3A catalytic site, J. Med. Chem. 50 (2007) 2886–2895.

[58] G.J. Finn, E. Kenealy, B.S. Creaven, D.A. Egan, In vitro cytotoxic potential and mechanism of action of selected coumarins, using human renal cell lines, Canc. Lett. 183 (2002) 61–68.

[59] F.A. Jimenez-Orozco, J.S. Lopez-Gonzalez, A. Nieto-Rodriguez, M.A. Velasco-Velazquez, J.A. Molina-Guarneros, N. Mendoza-Patino, M.J. Garcia-Mondragon, P. Elizalde-Galvan, F. Leon-Cedeno, J.J. Mandoki, Decrease of cyclin D1 in the human lung adenocarcinoma cell line A-427 by 7-hydroxycoumarin, Lung Canc. 34 (2001) 185–194.

[60] B. Thati, A. Noble, B.S. Creaven, M. Walsh, M. McCann, K. Kavanagh, M. Devereux, D.A. Egan, In vitro anti-tumour and cyto-selective effects of coumarin-3-carboxylic acid and three of its hydroxylated derivatives, along with their silver-based complexes, using human epithelial carcinoma cell lines, Canc. Lett. 248 (2007) 321–331.

[61] R.K. Singh, T.S. Lange, K.K. Kim, L. Brard, A coumarin derivative (RKS262) inhibits cell-cycle progression, causes pro-apoptotic signaling and cytotoxicity in ovarian cancer cells, Invest. N. Drugs 29 (2011) 63–72.

[62] M.A. Musa, V.L. Badisa, L.M. Latinwo, J. Cooperwood, A. Sinclair, A. Abdullah, Cytotoxic activity of new acetoxycoumarin derivatives in cancer cell lines, Anticancer Res. 31 (2011) 2017–2022.

[63] J. Bronikowska, E. Szliszka, D. Jaworska, Z.P. Czuba, W. Krol, The coumarin psoralidin enhances anticancer effect of tumor necrosis factor-related apoptosis-inducing ligand (TRAIL), Molecules 17 (2012) 6449–6464.

[64] S.U. Rehman, Z.H. Chohan, F. Gulnaz, C.T. Supuran, In-vitro antibacterial, antifungal and cytotoxic activities of some coumarins and their metal complexes, J. Enzym. Inhib. Med. Chem. 20 (2005) 333–340.

[65] V. Fernández-Moreira, M.L. Ortego, C.F. Williams, M.P. Coogan, M.D. Villacampa, M.C. Gimeno, Bioconjugated rhenium(I) complexes with amino acid derivatives: synthesis, photophysical properties, and cell imaging studies, Organometallics 31 (2012) 5950–5957.

[66] P. Kurz, B. Probst, B. Spingler, R. Alberto, Ligand variations in [ReX(diimine)(CO)$_3$] complexes: effects on photocatalytic CO$_2$ reduction, Eur. J. Inorg. Chem. (2006) 2966–2974, 2006.

[67] C.N. Morrison, K.E. Prosser, R.W. Stokes, A. Cordes, N. Metzler-Nolte, S.M. Cohen, Expanding medicinal chemistry into 3D space: metallofragments as 3D scaffolds for fragment-based drug discovery, Chem. Sci. 11 (2020) 1216–1225.

[68] F.G. Medina, J.G. Marrero, M. Macias-Alonso, M.C. Gonzalez, I. Cordova-Guerrero, A.G. Teissier Garcia, S. Osegueda-Robles, Coumarin heterocyclic derivatives: chemical synthesis and biological activity, Nat. Prod. Rep. 32 (2015) 1472–1507.

[69] J. Liu, Y.Q. Sun, Y. Huo, H. Zhang, L. Wang, P. Zhang, D. Song, Y. Shi, W. Guo, Simultaneous fluorescence sensing of Cys and GSH from different emission channels, J. Am. Chem. Soc. 136 (2014) 574–577.

[70] Z.-S. Wang, Y. Cui, K. Hara, Y. Dan-oh, C. Kasada, A. Shinpo, A high-light-harvesting-efficiency coumarin dye for stable dye-sensitized solar cells, Adv. Mater. 19 (2007) 1138–1141.

[71] M.E. Riveiro, N. De Kimpe, A. Moglioni, R. Vazquez, F. Monczor, C. Shayo, C. Davio, Coumarins: old compounds with novel promising therapeutic perspectives, Curr. Med. Chem. 17 (2010) 1325–1338.

[72] M. Tasior, D. Kim, S. Singha, M. Krzeszewski, K.H. Ahn, D.T. Gryko, π-Expanded coumarins: synthesis, optical properties and applications, J. Mater. Chem. C 3 (2015) 1421–1446.

[73] L. Huang, R. Zhang, Y. Hu, H. Zhou, J. Cao, H. Lv, S. Chen, S. Ding, G. Chen, Epidemiology and risk factors of methicillin-resistant Staphylococcus aureus and vancomycin-resistant enterococci infections in Zhejiang China from 2015 to 2017, Antimicrob. Resist. Infect. Contr. 8 (2019) 90.

[74] A.N. Neely, M.P. Maley, Survival of enterococci and staphylococci on hospital fabrics and plastic, J. Clin. Microbiol. 38 (2000) 724–726.

[75] S. Fijan, D. Pahor, S. Šostar Turk, Survival of Enterococcus faecium, Staphylococcus aureus and Pseudomonas aeruginosa on cotton, Textil. Res. J. 87 (2017) 1711–1721.

[76] C. Liu, A. Bayer, S.E. Cosgrove, R.S. Daum, S.K. Fridkin, R.J. Gorwitz, S.L. Kaplan, A.W. Karchmer, D.P. Levine, B.E. Murray, M.J. Rybak, D.A. Talan, H.F. Chambers, Clinical practice guidelines by the infectious diseases society of America for the treatment of methicillin-resistant Staphylococcus aureus infections in adults and children, Clin. Infect. Dis. 52 (2011) e18–e55.

[77] M.W. Pletz, O. Burkhardt, T. Welte, Nosocomial methicillin-resistant Staphylococcus aureus (MRSA) pneumonia: linezolid or vancomycin? - comparison of pharmacology and clinical efficacy, Eur. J. Med. Res. 15 (2010) 507–513.

[78] J.G. Hurdle, A.J. O'Neill, I. Chopra, R.E. Lee, Targeting bacterial membrane function: an underexploited mechanism for treating persistent infections, Nat. Rev. Microbiol. 9 (2011) 62–75.

[79] B. Jadoo, I.N. Booysen, M.P. Akerman, L. Rhyman, P. Ramasami, Novel coumarin rhenium(I) and -(V) complexes: formation, DFT and DNA binding studies, Polyhedron 144 (2018) 107–118.

[80] D.L. Higgins, R. Chang, D.V. Debabov, J. Leung, T. Wu, K.M. Krause, E. Sandvik, J.M. Hubbard, K. Kaniga, D.E. Schmidt, Q. Gao, R.T. Cass, D.E. Karr, B.M. Benton, P.P. Humphrey, Telavancin, a multifunctional lipoglycopeptide, disrupts both cell wall synthesis and cell membrane integrity in methicillin-resistant Staphylococcus aureus, Antimicrob. Agents Chemother. 49 (2005) 1127–1134.

[81] A. Pavic, N.D. Savic, B.D. Glisic, A. Crochet, S. Vojnovic, A. Kurutos, D.M. Stankovic, K.M. Fromm, J. Nikodinovic-Runic, M.I. Djuran, Silver(I) complexes with 4,7-phenanthroline efficient in rescuing the zebrafish embryos of lethal Candida albicans infection, J. Inorg. Biochem. 195 (2019) 149–163.

[82] A. Pavic, B.D. Glisic, S. Vojnovic, B. Warzajtis, N.D. Savic, M. Antic, S. Radenkovic, G.V. Janjic, J. Nikodinovic-Runic, U. Rychlewska, M.I. Djuran, Mononuclear gold(III) complexes with phenanthroline ligands as efficient inhibitors of angiogenesis: a comparative study with auranofin and sunitinib, J. Inorg. Biochem. 174 (2017) 156–168.

[83] L. Senerovic, M.D. Zivkovic, A. Veselinovic, A. Pavic, M.I. Djuran, S. Rajkovic, J. Nikodinovic-Runic, Synthesis and evaluation of series of diazine-bridged dinuclear platinum(II) complexes through in vitro toxicity and molecular modeling: correlation between structure and activity of Pt(II) complexes, J. Med. Chem. 58 (2015) 1442–1451.

[84] C. Chakraborty, C.H. Hsu, Z.H. Wen, C.S. Lin, G. Agoramoorthy, Zebrafish: a complete animal model for in vivo drug discovery and development, Curr. Drug Metabol. 10 (2009) 116–124.

[85] C.A. MacRae, R.T. Peterson, Zebrafish as tools for drug discovery, Nat. Rev. Drug Discov. 14 (2015) 721.

[86] S. Basu, C. Sachidanandan, Zebrafish: a multifaceted tool for chemical biologists, Chem. Rev. 113 (2013) 7952–7980.

[87] V. Torraca, S. Mostowy, Zebrafish infection: from pathogenesis to cell biology, Trends Cell Biol. 28 (2018) 143–156.

[88] T.K. Prajsnar, V.T. Cunliffe, S.J. Foster, S.A. Renshaw, A novel vertebrate model of Staphylococcus aureus infection reveals phagocyte-dependent resistance of zebrafish to non-host specialized pathogens, Cell Microbiol. 10 (2008) 2312–2325.

[89] D. Milivojevic, N. Sumonja, S. Medic, A. Pavic, I. Moric, B. Vasiljevic, L. Senerovic, J. Nikodinovic-Runic, Biofilm-forming ability and infection potential of Pseudomonas aeruginosa strains isolated from animals and humans, Pathog. Dis. 76 (2018).

[90] E. Zaccaria, R. Cao, J.M. Wells, P. van Baarlen, A zebrafish larval model to assess virulence of porcine Streptococcus suis strains, PloS One 11 (2016), e0151623.

[91] P.Y. Lam, R.T. Peterson, Developing zebrafish disease models for in vivo small molecule screens, Curr. Opin. Chem. Biol. 50 (2019) 37–44.

[92] A. Ordas, R.-J. Raterink, F. Cunningham, H.J. Jansen, M.I. Wiweger, S. Jong-Raadsen, S. Bos, R.H. Bates, D. Barros, A.H. Meijer, R.J. Vreeken, L. Ballell-Pages, R.P. Dirks, T. Hankemeier, H.P. Spaink, Testing tuberculosis drug efficacy in a zebrafish high-throughput translational medicine screen, Antimicrob. Agents Chemother. 59 (2015) 753.

[93] T.K. Prajsnar, R. Hamilton, J. Garcia-Lara, G. McVicker, A. Williams, M. Boots, S.J. Foster, S.A. Renshaw, A privileged intraphagocyte niche is responsible for disseminated infection of Staphylococcus aureus in a zebrafish model, Cell Microbiol. 14 (2012) 1600–1619.

[94] G.M. Sheldrick, SHELXT - integrated space-group and crystal-structure determination, Acta Crystallogr. A 71 (2015) 3–8.

[95] G.M. Sheldrick, Crystal structure refinement with SHELXL, Acta Crystallogr. C 71 (2015) 3–8.

[96] J.D. Chai, M. Head-Gordon, Long-range corrected hybrid density functionals with damped atom-atom dispersion corrections, Phys. Chem. Chem. Phys. 10 (2008) 6615–6620.

[97] J.D. Chai, M. Head-Gordon, Systematic optimization of long-range corrected hybrid density functionals, J. Chem. Phys. 128 (2008), 084106.

[98] S. Grimme, Semiempirical GGA-type density functional constructed with a long-range dispersion correction, J. Comput. Chem. 27 (2006) 1787–1799.

[99] A.D. Becke, Density-functional thermochemistry. V. Systematic optimization of exchange-correlation functionals, J. Chem. Phys. 107 (1997) 8554–8560.

[100] Q. Wu, W. Yang, Empirical correction to density functional theory for van der Waals interactions, J. Chem. Phys. 116 (2002) 515–524.

[101] D. Andrae, U. Häußermann, M. Dolg, H. Stoll, H. Preuß, Energy-adjustedab initio pseudopotentials for the second and third row transition elements, Theor. Chim. Acta 77 (1990) 123–141.

[102] M.B. Hansen, S.E. Nielsen, K. Berg, Re-examination and further development of a precise and rapid dye method for measuring cell growth/cell kill, J. Immunol. Methods 119 (1989) 203–210.

[103] N.D. Savic, S. Vojnovic, B.D. Glisic, A. Crochet, A. Pavic, G.V. Janjic, M. Pekmezovic, I.M. Opsenica, K.M. Fromm, J. Nikodinovic-Runic, M.I. Djuran, Mononuclear silver(I) complexes with 1,7-phenanthroline as potent inhibitors of Candida growth, Eur. J. Med. Chem. 156 (2018) 760–773.

[104] OECD, Test No. 236: Fish Embryo Acute Toxicity (FET) Test, OECD Guidelines for the Testing of Chemicals, Section 2, OECD, 2013.

[105] J.-H. He, S.-Y. Guo, F. Zhu, J.-J. Zhu, Y.-X. Chen, C.-J. Huang, J.-M. Gao, Q.-X. Dong, Y.-X. Xuan, C.-Q. Li, A zebrafish phenotypic assay for assessing drug-induced hepatotoxicity, J. Pharmacol. Toxicol. Methods 67 (2013) 25–32.